

Wave processes in a viscous shock layer and control of fluctuations

A. A. MASLOV^{1,2}, S. G. MIRONOV^{1,2}, A. N. KUDRYAVTSEV^{1,2},
T. V. POPLAVSKAYA^{1,2}† AND I. S. TSYRYULNIKOV^{1,2}

¹Khristianovich Institute of Theoretical and Applied Mechanics, Novosibirsk 630090, Russia

²Department of Physics, Novosibirsk State University, Novosibirsk 630090, Russia

(Received 13 January 2009; revised 17 November 2009; accepted 17 November 2009;
first published online 18 March 2010)

Generation and development of disturbances in a hypersonic viscous shock layer on a flat plate is studied both experimentally and numerically. The study is performed at the Mach number $M_\infty = 21$ and the Reynolds number $Re_L = 1.44 \times 10^5$ and is aimed at elucidating the physical mechanisms that govern the receptivity and instability of the shock layer at extremely high hypersonic velocities. The experiments are conducted in a hypersonic nitrogen-driven wind tunnel. An electron-beam fluorescence technique, a Pitot probe and a piezoceramic transducer are used to measure the mean density and Mach number contours, as well as density and pressure fluctuations, their spectra and spatial distributions in the shock layer. Direct numerical simulations are performed by solving the Navier–Stokes equations with a high-order shock-capturing scheme in a computational domain including the leading and trailing edges of the plate, so that the bow shock wave and the wake behind the plate are also simulated. It is demonstrated that computational and experimental data characterizing the mean flow field, intensity of density fluctuations and their spatial distributions in the shock layer are in close agreement. It is found that excitation of the shock layer by external acoustic waves leads to generation of entropy–vortex disturbances with two maxima of density fluctuations: directly behind the shock wave and on the external edge of the boundary layer. At the same time, the pressure fluctuations decay inward into the shock layer, away from the shock, which agrees with the linear theory of interaction of shock waves with small perturbations. Thus, the entropy–vortex disturbances are shown to dominate in the hypersonic shock layer at very high Mach numbers, in contrast with the boundary layers at moderate hypersonic velocities where acoustic modes are most important. A parametric numerical study of wave processes in the shock layer induced by external acoustic waves is performed with variations of frequency, amplitude and angle of propagation of external disturbances. The amplitude of generated disturbances is observed to grow and decay periodically along the streamwise coordinate, and the characteristics of these variations depend on the frequency and direction of incident acoustic waves. The hypersonic shock layer excited by periodic blowing and suction near the leading edge is also investigated; in the experiments, this type of excitation is obtained by using an oblique-cut whistle. It is shown that blowing/suction generates disturbances resembling those generated by external acoustic waves, with similar spatial distributions and phase velocities. This result paves the way for active control of instability development in the shock layer by means of destructive interference of two types of disturbances. Numerical simulations

† Email address for correspondence: popla@itam.nsc.ru

are performed to show that instability waves can be significantly amplified or almost entirely suppressed, depending on the relative phase of blowing/suction and acoustic disturbances. Wind-tunnel experiments completely confirm this numerical prediction. Thus, the feasibility of delaying instability development in the hypersonic shock layer has been demonstrated for the first time.

1. Introduction

The flow around the elements of a vehicle flying at a hypersonic velocity in the upper atmosphere can occur in several flow regimes (figure 1). In the flow region near the leading edges, the boundary layer and the shock wave interact and merge, so that it is impossible to indicate a clear boundary between them. The merged layer gradually transforms to the region of strong viscous–inviscid interaction. In the region of strong interaction, the inviscid flow between the shock wave and the boundary layer either is small or cannot be identified at all. Then there follows the regime of weak viscous–inviscid interaction where the inviscid flow plays an important role. The regimes of the merged layer and strong interaction can be united and considered together as the regime of a viscous shock layer.

A viscous shock layer is always formed on the leading edges of hypersonic flying vehicles, where the local Reynolds number is not yet too high and viscous forces dominate in the flow behind the bow shock wave. The length of this layer depends on flow conditions. For instance, for an aeroplane flying with a velocity corresponding to a Mach number of 12 at an altitude of 60 km, the viscous shock layer extends for 1 m from the leading edge. Perturbations formed in the shock layer propagate in the downstream direction and affect the evolution of fluctuations and the laminar-turbulent transition in the hypersonic boundary layer of the flying vehicle as a whole. The latter influences the friction drag, aerodynamic characteristics and magnitude and distribution of heat fluxes over the aeroplane surface.

The analysis of the laminar-turbulent transition in the boundary layer is usually started from the problem of receptivity, i.e. excitation of waves by external perturbations. For hypersonic flows, two cases of disturbance excitation in the viscous shock layer can be identified: continuous (distributed) generation in an extended flow region and localized generation under an action localized in space. Generation of instability waves by acoustic perturbations of the external flow is an example of distributed generation of fluctuations in the shock layer, whereas generation of instability waves by means of periodic blowing/suction perturbations on the body surface near the leading edge can be considered as an example of localized generation.

The characteristics of disturbances in a hypersonic shock layer are determined by the following basic processes: action of external flow perturbations on the shock layer, generation of fluctuations inside the shock layer (receptivity) and development of fluctuations because of their downstream convection. These processes are interrelated; they proceed simultaneously over the entire shock layer and can be considered as a unified mechanism of distributed receptivity. Morkovin (1968) offered the clearest formulation of the receptivity problem. Receptivity is an important initial stage of the laminar-turbulent transition in the boundary layer. Affecting flow receptivity is one of the possible methods of controlling the laminar-turbulent transition in high-velocity flows, which were reviewed by Kimmel (2003). Profound theoretical investigations of the receptivity of supersonic and moderately hypersonic boundary layers to external disturbances were performed by Ma & Zhong (2003*a,b*, 2005), Fedorov & Tumin

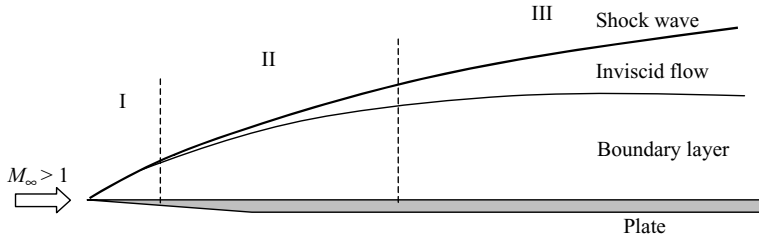


FIGURE 1. Hypersonic flow past a flat plate: I, merged layer; II, strong viscous–inviscid interaction; III, weak viscous–inviscid interaction.

(2004) and Tumin (2006, 2007), and the receptivity to disturbances introduced from the surface was studied by Egorov, Sudakov & Fedorov (2004) and Wang & Zhong (2005). It seems of interest to extend the study to extremely high hypersonic velocities and investigate the receptivity of a hypersonic shock layer to external flow oscillations and to perturbations induced by surface sources and to develop methods for controlling the intensity of fluctuations arising in the shock layer.

This problem has not been adequately studied yet. Scarce experimental investigations of the wave processes in the hypersonic shock layer were started in the 1960s and were virtually interrupted in the early 1970s. The main results of these activities were summarized by Harwey & Bushnell (1969), Wallace (1969), Beckwith, Harvey & Clark (1971), Fisher *et al.* (1971), Kemp & Owen (1972) and Smith & Driscoll (1975). Sporadic data were obtained in those studies on the distributions of integral characteristics of fluctuations of the mass flow, density and temperature in the shock layer and in the hypersonic mixing layer for moderate unit Reynolds numbers in the range of Mach numbers $M_\infty = 7\text{--}43$. The measurements were usually performed for natural disturbances of the flow in the shock layer on the nozzle surface or on the test-section wall in hypersonic nitrogen- or helium-driven wind tunnels. These data could be hardly interpreted from the viewpoint of receptivity and stability problems because the field of fluctuations was affected by the entire history of the gas flow in the boundary layer on the nozzle and test-section walls, and the measurements were performed by methods developed for low-velocity high-density flows.

It was only after a method was developed for measuring all wave characteristics of density fluctuations in a low-density hypersonic flow (Mironov & Maslov 2000*a*) that a targeted research of wave processes in the hypersonic viscous shock layer became possible. The characteristics of density fluctuations in the shock layer on a flat plate, sharp cone and curved compression surface and in the wake flow were recently measured by a non-intrusive method of electron-beam fluorescence of nitrogen in a flow with a Mach number $M_\infty = 21$ and unit Reynolds number $Re_{1\infty} = 6 \times 10^5 \text{ m}^{-1}$ (Maslov & Mironov 1999; Mironov & Maslov 2000*a, b*; Mironov & Aniskin 2004; Maslov, Mironov & Aniskin 2005). This method allowed the mean density field, the spectra and the phase velocity of density fluctuations in the shock layer to be measured and the growth rate of disturbances to be estimated. The method of artificial wave packets was applied to low-density hypersonic flows for the first time by Mironov & Maslov (2000*b*).

The method of wave packets for modelling the action of both external and internal perturbations on the shock layer allows one to obtain data on the wave characteristics of disturbances in the shock layer and to compare them with available mathematical models of the processes. It also implies development, fabrication and application

of sources of periodic perturbations with a controlled amplitude and phase. Such sources have been developed and are used in studying stability of subsonic and supersonic boundary layers. Numerous references and descriptions of various devices designed for generating periodic perturbations in a subsonic external flow and in the boundary layer can be found in Boiko *et al.* (2002). A spark discharge in the chamber is frequently used for supersonic flows (Kosinov, Maslov & Shevelkov 1990). This method is widely known by the name ‘synthetic jets’. For low-density hypersonic flows, the most suitable source of periodic perturbations was found to be an oblique-cut gas-dynamic whistle (Maslov & Mironov 1996).

It is difficult to construct a holistic pattern of the wave processes in the shock layer because the parametric studies in hypersonic wind tunnels are extremely complicated and only a limited number of parameters can be measured. On the other hand, understanding the mechanisms of the emergence and evolution of disturbances in the shock layer and their hierarchy and relationships is necessary to choose an effective method for controlling the disturbances.

To overcome these difficulties, it seems reasonable to use a comprehensive numerical and experimental approach to study the hypersonic shock layer. Numerical simulations offer the possibility of a large-scale parametric study of the flow and obtaining data on all flow parameters, while experimental data are important for validation of the mathematical model and numerical algorithm.

In computations, it is necessary to use adequate (with respect to flow conditions) mathematical models and numerical simulation methods. The viscous shock layer has some specific features distinguishing it from the boundary layer. In the case of a hypersonic shock layer, the flow is not parallel; significant divergence of the flow and a streamwise pressure gradient are observed; the bow shock wave is located rather close to the boundary layer; and instability waves can be excited not only through the receptivity mechanism but also because of direct amplification of perturbations passing through the shock wave. The most famous and well-developed models of the wave processes in supersonic boundary layers are the locally parallel linear theory of stability (Mack 1975; Gaponov & Maslov 1980) and parabolized equations of stability (Bertolotti & Herbert 1991; Chang *et al.* 1991). These models have demonstrated appreciable advantages in studying flows with weak viscous–inviscid interaction.

In the hypersonic shock layer, however, the bow shock wave is so close to the body surface that the transverse sizes of the shock and boundary layers are commensurable. In this case, it is necessary to take into account the influence of the shock wave and viscous–inviscid interaction on stability characteristics. The boundary conditions for disturbances on the shock wave were derived from the linearized Rankine–Hugoniot conditions (Chang, Malik & Hussaini 1990; Maslov *et al.* 2004a; Maslov, Poplavskaya & Smorodsky 2004b). It was demonstrated that reflection of disturbances from the shock wave results in branching of the solutions of the linear stability problem; i.e. more than one solution was obtained for a comparatively narrow range of frequencies. The best agreement between the disturbance growth rates computed by the linear stability theory and measured in experiments was observed if the mean flow was computed with the use of parabolized Navier–Stokes equations.

The use of direct numerical simulations (DNSs) on the basis of the full unsteady Navier–Stokes equations is the most promising approach in this case. It allows abandoning the simplifying assumptions of the boundary-layer model and obtaining steady and unsteady flow fields directly. The DNS approach was successfully used for simulating the disturbances in the hypersonic boundary layer (Zhong 2000, 2001; Ma & Zhong 2004; Wang & Zhong 2005; Egorov, Sudakov & Fedorov 2006a,b, 2008;

Tumin, Wang & Zhong 2007). As the experience gained in these studies has shown, application of the linear stability theory facilitates interpretation of the research results.

In addition to understanding the processes of receptivity and evolution of disturbances in hypersonic shock layers, the goal of these experimental and numerical studies was to develop methods and devices for controlling the intensity of fluctuations. This problem is an important step in controlling the laminar-turbulent transition. The problem of disturbance control can be solved by various methods, which were systematized and reviewed by Gad-el-Hak (1996). All methods of affecting the evolution of disturbances can be classified into two large groups: passive and active. In passive methods, the object to be controlled is the mean flow; changes in the parameters of the mean flow interrupt the growth of disturbances in the boundary layer and lead to their suppression. These methods are usually energy consuming because it is necessary to change the parameters of large masses of the gas flowing in the boundary layer. In active methods, the action is applied to the disturbances directly, which alters the disturbance amplitude. The energy consumption in these methods is lower because the energy of fluctuations at the beginning of their development is only a small fraction of the energy of the mean flow in the boundary layer. An important issue is the correct choice of methods, which is determined by flow velocity. Active methods are successfully used in subsonic flows: blowing/suction, microelectromechanical systems (MEMS), local periodic heating and electric discharge (Biringen 1984; Nosenchuck 1988; Gaster 2000; Moreau 2007). Some of these methods of active control (periodic blowing/suction, electric discharge and synthetic jets) were also used for supersonic and hypersonic boundary layers; in addition, specific methods of active flow control were developed (see Kimmel 2003). In particular, the method of absorbing acoustic perturbations by a sound-absorbing coating was successfully used for hypersonic flows (Fedorov *et al.* 2001, 2003); this method can also be considered as an active control method. An analysis of the literature (Biringen 1984; Nosenchuck 1988; Gad-el-Hak 1996; Gaster 2000; Fedorov *et al.* 2001, 2003; Moreau 2007) shows that the choice of the method of active control of disturbances in the boundary layer is determined by mean flow parameters and by the type of the disturbance mode. An optimal method for controlling the hypersonic shock layer should also be determined. For example, based on the results of studying the receptivity of the shock layer to external acoustic waves (Kudryavtsev *et al.* 2006; Maslov *et al.* 2007), an interference method of controlling disturbances in the shock later was successfully used (Fomin *et al.* 2007; Maslov *et al.* 2008).

The present paper reports the results of a numerical and experimental study of the distributed and localized receptivity of a hypersonic viscous shock layer on a flat plate at a zero angle of attack, flow Mach number $M_\infty = 21$, unit Reynolds number $Re_{1\infty} = 6 \times 10^5 \text{ m}^{-1}$ and temperature factor of the surface varied from 0.08 to 0.5. The majority of experimental results were obtained by the method of wave packets. The numerical study was performed by the method of DNSs of disturbances, based on two-dimensional unsteady Navier–Stokes equations. With the data obtained, controlling the intensity of disturbances in a hypersonic shock layer on a flat plate was modelled numerically and experimentally.

2. Experimental equipment and diagnostic methods

2.1. Hypersonic wind tunnel

The experiments were performed in a T-327A hypersonic nitrogen-driven wind tunnel based at the Khristianovich Institute of Theoretical and Applied Mechanics (Siberian

Branch, Russian Academy of Sciences). This is a free-jet wind tunnel with a running time of 40 s. The exit diameter of the wind-tunnel nozzle is 220 mm; the flow Mach number at the exit of a conical nozzle is 20; and the diameter of a uniform flow core is 0.1 m. Owing to jet expansion in the wind-tunnel test section, the flow Mach number increases by three units per metre, so that it reaches $M_\infty \cong 21$ in the region of measurements. The experiments were performed with a fixed unit Reynolds number $Re_{1\infty} = 6 \times 10^5 \text{ m}^{-1}$ and stagnation temperature $T_0 = 1200 \text{ K}$. Under these conditions, the uniform flow core diameter was 0.1 m. At this stagnation temperature, a significant part of nitrogen molecules in the settling chamber are vibrationally excited. Relaxation of vibrational excitation, which occurs during flow expansion and cooling, is terminated when the flow Mach number approaches $\cong 15$ because of an insufficient number of intermolecular collisions. As a result, the level of vibrational excitation of molecules in the wind-tunnel test section corresponds to a temperature of $\cong 26 \text{ K}$. The gas in the shock layer on the plate is heated to the maximum temperature of $\cong 400 \text{ K}$ (see the data in §4); however, the total number of intermolecular collisions during the gas motion through the shock layer is not sufficient to put the vibrational temperature in equilibrium with the translational and rotational degrees of freedom. Therefore, the vibrational temperature of nitrogen molecules remains substantially lower than the kinetic temperature of the gas in the shock layer, which allows one to neglect its influence on wave processes.

2.2. Flat-plate model

The flat plate was made of low-carbon steel. Its planform was a trapezoid with a length of 240 mm, width at the leading edge of 100 mm and width at the trailing edge of 80 mm. The plate thickness was 8 mm; the sharp leading edge of the plate was shaped as a 7° wedge with a bluntness radius of $\cong 0.05 \text{ mm}$. The side edges of the plate were also wedges with an angle of 20° . The surface temperature was equal to 300 K and was monitored by a copper–constantan thermocouple. The flat plate was mounted at a zero angle of attack to the flow direction. In the paper, we use a Cartesian coordinate system whose origin coincides with the plate leading edge; the x axis is aligned with the streamwise axis of the plate; the y axis is normal to the plate surface; and the z axis is aligned in the spanwise direction.

Along the streamwise axis of the plate, at a distance of 70 mm from the leading edge, there was a flush-mounted graphite insert 170 mm long, 15 mm wide and 5 mm thick (see figure 2). Graphite and steel have approximately identical values of thermal diffusivity, which minimized the distortion of the temperature field on the plate surface. The insert was used to absorb the probing beam in the experiment arrangement with the electron beam incident normal on to the plate surface.

2.3. Diagnostic methods

The parameters measured in wind-tunnel experiments were the mean density and density fluctuations, steady-state pressure and pressure fluctuations behind the normal shock wave. The steady-state pressure behind the normal shock was measured by a Pitot tube, and the pressure fluctuations were measured by a piezoceramic transducer of pressure fluctuations. In processing the Pitot measurements, a correction was made for flow rarefaction, in accordance with Beckwith *et al.* (1971) and Roger, Wainright & Touryan (1966).

The mean density and density fluctuations were measured by the method of electron-beam fluorescence. This method adapted to measurements of the characteristics of density fluctuations (spectrum and phase of fluctuations, phase velocity of disturbances) was described in detail by Mironov & Maslov (2000a). The method was used in the experiment arrangement with the electron beam directed parallel to the

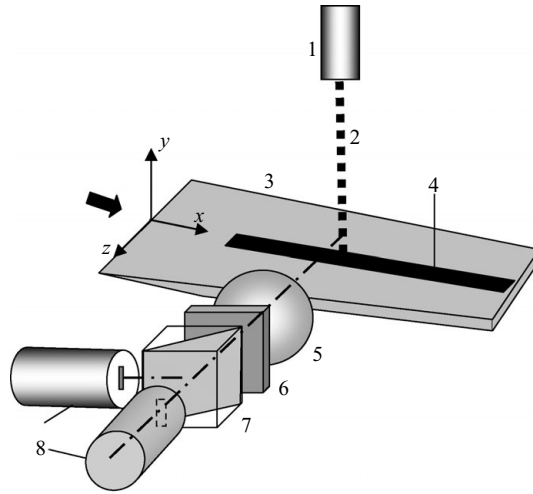


FIGURE 2. Electron-beam measurements: 1, electron gun; 2, electron beam; 3, flat plate; 4, graphite insert; 5, lens; 6, light filter; 7, light splitter; 8, photoamplifiers with aperture diaphragms.

model surface (Maslov & Mironov 1999; Mironov & Maslov 2000*a,b*; Mironov & Aniskin 2004; Maslov *et al.* 2005). In the present experiments, the method was slightly modified. The probing electron beam was incident normal on to the graphite insert in the plate surface, which absorbed the beam and minimized the flux of secondary electrons. The measurements in quiescent nitrogen showed that the intensity of gas fluorescence induced by secondary electrons even in the near vicinity of the surface was within 10% of the fluorescence caused by the primary electron beam. A normally incident electron beam passed high-density regions on the minimum length and became weakly scattered, which made the measurements more local and allowed the scattering of the probing beam electrons to be considered as a second-order effect. For this reason, it was possible to take into account only the process of collisional deactivation of electron-excited molecules, substantially simplify the calculations of the mean density and density fluctuations and improve the measurement accuracy. The procedure of determining the mean density and density fluctuations here was similar to measurements in the wake flow described by Aniskin & Mironov (2000); the remaining features of the measurement procedure were consistent with the basic technique (Mironov & Maslov 2000*a*). The flow was probed with an electron beam; the electron energy was 14 keV with a current strength in the beam equal to 0.5 mA; the beam diameter in vacuum was 1 mm. The density fluctuations were measured in the frequency range of 1–50 kHz.

2.4. Methods of generating controlled periodic perturbations

2.4.1. Introduction of periodic perturbations into the shock layer from the plate surface

Perturbations were introduced into the shock layer on the flat plate by a cylindrical oblique-cut gas-dynamic whistle (Maslov & Mironov 1996). This whistle is a copper cylinder closed on one side and is cut at an angle of 40° to the centreline. The cylinder contains a piston with a transducer of pressure fluctuations, which can be moved to change the oscillation frequency. The whistle was mounted under the plate close to its leading edge, as is shown in figure 3.

In such a configuration, pressure oscillations arise in the whistle resonator. They introduce a pressure pulse into the shock layer in the phase of gas exhaustion from

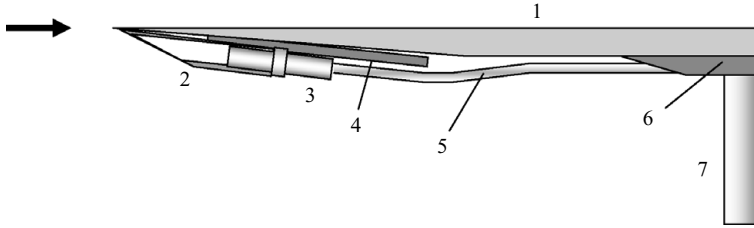


FIGURE 3. Arrangement of the whistle on the flat plate: 1, plate; 2, whistle; 3, transducer of pressure fluctuations; 4, heat-removing plate; 5, transducer cable; 6, heat insulation; 7, sting of the plate.

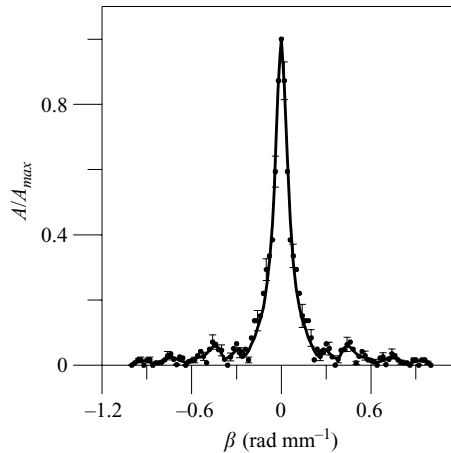


FIGURE 4. Spanwise spectrum of density fluctuations induced in the shock layer on a flat plate by an oblique whistle ($x = 75$ mm; $y = 13$ mm).

the resonator, while the bulk of the gas escaping from the resonator flows under the plate. The oblique-cut whistle had been already used for introducing perturbations into the shock layer (Mironov & Maslov 2000*b*; Mironov & Aniskin 2004), but the mean flow on the flat plate in the present experimental configuration was much less distorted than the flow in those publications, and the procedure of variation of the amplitude of perturbations introduced into the flow was substantially simplified. The flow field distortion in this arrangement was less than 10% in terms of density and less than 2.5% in terms of velocity. The signal of the transducer of pressure fluctuations was used to identify artificial perturbations on the background of natural noise of the flow and to determine the phase of fluctuations. The transverse size of the steady perturbed region of the mean flow was 10 mm on the plate leading edge and increased linearly in the downstream direction with an expansion angle of $\cong 5^\circ$. The region of periodic density fluctuations had a similar configuration.

The amplitude and phase of density fluctuations generated in the shock layer with the whistle were measured along the z coordinate at those positions at which the maximum amplitude of fluctuations in the y direction was reached. The measurements were repeated in several x cross-sections. Expansion of density fluctuations into a spectrum with respect to spanwise wavenumbers β (β -spectrum) shows that the spectrum has only one finite-width peak at a zero wavenumber (figure 4). As the measurements along the z axis were performed within the limits of the maximum

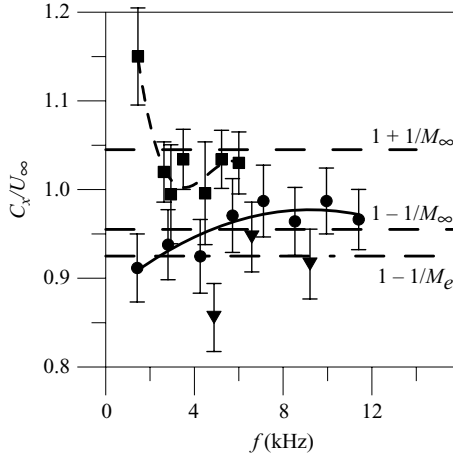


FIGURE 5. Streamwise phase velocity of disturbances in the flow versus the frequency: squares, disturbances generated by a spark discharge; circles, natural disturbances of the flow; inverted triangles, disturbances generated by the whistle (Aniskin & Mironov 2000).

plate width ($z = \pm 50$ mm), the spectral resolution was restricted by the value of $0.0314 \text{ rad mm}^{-1}$. The phase of density fluctuations is constant within this peak. It means that the waves propagating in the shock layer are two-dimensional. Noticeable expansion of the peak base is caused by the fact that periodic perturbations introduced into the shock layer propagate in a band $\cong 10$ mm wide, and expansion with respect to harmonic functions gives rise to additional spectral components with high wavenumbers. Direct measurements of density fluctuations on the plate in the plane (x, z) show that the perturbations introduced by the whistle are really two-dimensional waves propagating in a finite-width channel.

The oblique-cut whistle was definitely demonstrated to generate acoustic perturbations of the slow mode in a hypersonic flow ($M_\infty = 5$) (Tsyryulnikov & Mironov 2005). The perturbations generated in the hypersonic flow ($M_\infty = 21$) by the whistle (Maslov, Mironov & Aniskin 2005) (inverted triangles in figure 5) may probably be acoustic perturbations of the slow mode, though the experimental measurements are too scarce for a definitive conclusion. The measured phase velocities C_x are below $C_x = 1$ and close to the value $C_x = 1 - 1/M_e$, where M_e is the flow Mach number behind the bow shock wave generated by the oblique-cut whistle.

2.4.2. Introduction of periodic perturbations into the external flow

Periodic acoustic perturbations were generated in the hypersonic flow by a powerful periodic spark discharge in the settling chamber of the wind tunnel. The spark discharge was triggered by an electric pulse, which served as a reference signal for identifying the periodic disturbances on the background of natural noise of the wind-tunnel flow. It was shown by Tsyryulnikov & Mironov (2005) that pressure oscillations in the settling chamber generated fast-mode acoustic waves in the hypersonic ($M_\infty = 5$) flow. The wave characteristics of disturbances induced in the hypersonic flow of the T-327A wind tunnel by an electric spark in the settling chamber were measured in the present work. In particular, a piezoceramic transducer measured the streamwise distributions of the amplitude and phase of acoustic fluctuations of pressure at a length of 0.15 m and their cross-streamwise distributions within the uniform core flow in the wind-tunnel test section. As an example, figure 6 shows the β -spectrum of flow

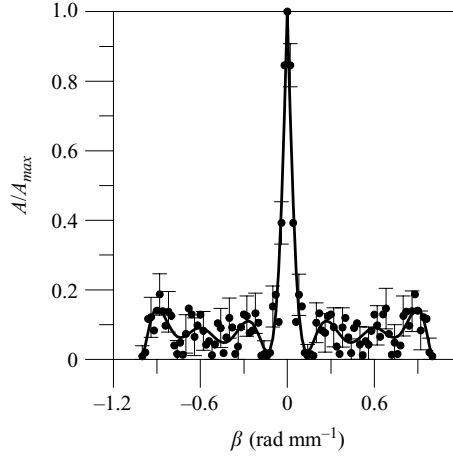


FIGURE 6. Spanwise spectrum of pressure fluctuations generated in the free stream by a spark discharge at a frequency of 13 kHz ($x=0$, $y=0$).

disturbances measured along the plate leading edge. The resolution of the β -spectrum is $0.0314 \text{ rad mm}^{-1}$. The spectrum has a narrow peak at a zero wavenumber, which evidences propagation of two-dimensional waves along the flow. The spectral regions outside the peak are most probably noise components of the spectrum. The measured streamwise distributions of the phase of pressure fluctuations C_x (squares in figure 5) are scattered significantly. For this reason, we cannot definitely conclude that the flow disturbances are fast-mode acoustic waves, as it was clearly shown for $M_\infty = 5$ by Tsyryulnikov & Mironov (2005).

2.4.3. Natural disturbances of the wind-tunnel flow

Natural disturbances compose the inherent noise of the wind-tunnel flow. The characteristics of natural disturbances of the hypersonic flow in the T-327A wind tunnel were measured in the present work. As these flow disturbances are randomly distributed in time, the reference signal for phase measurements was the variable component of the signal of the electron-beam fluorescence of the flow in the wind-tunnel test section, which was related to density fluctuations in the flow. In this case, the electron beam was non-scanning and passed through the flow axis. A movable piezoceramic transducer of pressure fluctuations located at a certain distance downstream from the electron beam measured the distributions of the amplitude and phase of pressure fluctuations in the streamwise direction over a length of 0.15 m and across the flow within the uniform core flow. High spatial coherence of natural disturbances was found. A possible reason is the effect of a small space angle at which the region of the emergence of disturbances is observed from the measurement region (Born & Wolf 1968). Most probably, the disturbances in the flow are formed in a small-size region near the nozzle throat, where flow instability in the boundary layer on the nozzle wall arises.

Spatial coherence of natural disturbances in the wind-tunnel flow made it possible to obtain the spectra of pressure fluctuations as functions of the transverse wavenumber and to measure the distributions of the fluctuation phase over the streamwise coordinate. As an example, figure 7 shows the spanwise spectrum measured along the leading edge of the plate, which has a narrow peak at a zero wavenumber, evidencing propagation of two-dimensional waves in the streamwise direction. It is most likely

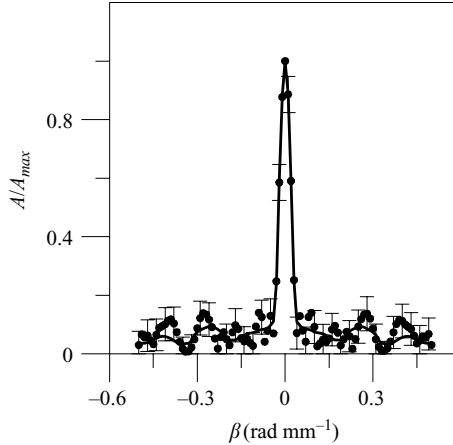


FIGURE 7. Spanwise spectrum of natural pressure fluctuations in the free stream for a frequency of $f = 13$ kHz ($x = 0$, $y = 0$).

that the spectrum portions outside the peak are noise. The β -spectrum resolution is 0.0314 rad mm^{-1} .

The measurements of the relative phase as a function of the streamwise coordinate showed that natural disturbances in the flow propagated with a phase velocity close to that of slow acoustic waves $C_x = 1 - 1/M_\infty$ (circles in figure 5). This result agrees with the data obtained previously for acoustic disturbances in supersonic wind tunnels (Laufer 1964; Tsyryulnikov & Mironov 2005). It was shown in Laufer (1964) that acoustic disturbances were generated by Mach waves. These waves arise owing to interaction of the supersonic flow with hydrodynamic disturbances of the boundary layer on the wind-tunnel walls, which are entrained in the downstream direction with a velocity lower than that of the main supersonic flow. Mach waves are generated in the flow if the difference in velocities is greater than the velocity of sound. Correspondingly, acoustic disturbances generated by these waves in the wind tunnel move downstream with a velocity $u - c$, where u is the flow velocity and c is the local velocity of sound.

The spectrum of natural fluctuations of density in the free stream was measured by the method of electron-beam fluorescence. It is an exponentially decreasing dependence on frequency (figure 8). The major fraction of the fluctuations lies in the frequency range $f = 0$ – 13 kHz. The level of the normalized integral density fluctuations ρ'/ρ_∞ in the uniform core flow in this range is $\cong 1.4\%$.

To conclude this section, a few words concerning the angles of propagation of disturbances in the flat-plate shock layer should be said. Data on the angles of propagation of natural density disturbances in the shock layer obtained by direct measurements of the streamwise and normal phase velocities were presented by Mironov & Maslov (2000a) and Maslov *et al.* (2005). It was shown that the angle of propagation is smaller than 5° with respect to the flow direction on the boundary-layer edge for frequencies $f > 7$ kHz; therefore, these disturbances can be considered as two-dimensional.

3. Governing equations and numerical method

It is well known (Gaponov & Maslov 1980) that the most unstable disturbances in boundary layers at high Mach numbers are those propagating at a zero angle to the

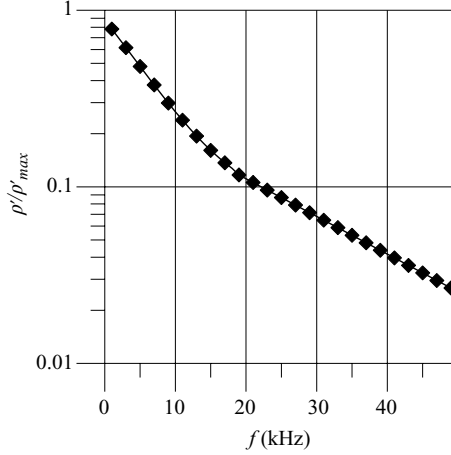


FIGURE 8. Free-stream spectrum of density fluctuations averaged over the uniform core flow.

basic flow direction. This means that the flow remains two-dimensional at the early stages of the transition to turbulence. The above-described experiments performed at the Mach number $M_\infty = 21$ also showed that two-dimensional waves prevailed both in the free stream and in the shock layer on the flat plate. However, the base flow behind the plate trailing edge, which is of small but finite thickness and of finite spanwise size, seems to be three-dimensional. Nevertheless, the upstream influence of the three-dimensional base flow is limited only by an immediate vicinity of the trailing edge and does not affect the boundary layer over most of the plate surface. Numerical simulations in the present work were not aimed at investigating these minor three-dimensional effects; therefore, two-dimensional Navier–Stokes equations were solved. They were written in the conservative form as

$$\frac{\partial \mathbf{Q}}{\partial t} + \frac{\partial \mathbf{F}}{\partial x} + \frac{\partial \mathbf{G}}{\partial y} = \frac{M_\infty}{Re_L} \left(\frac{\partial \mathbf{F}^v}{\partial x} + \frac{\partial \mathbf{G}^v}{\partial y} \right). \quad (1)$$

Here t is the time; x and y are the coordinates along and across the plate; \mathbf{Q} is the vector of conservative variables; \mathbf{F} and \mathbf{G} are the vectors of inviscid fluxes; and \mathbf{F}^v and \mathbf{G}^v are the vectors of viscous fluxes:

$$\left. \begin{aligned} \mathbf{Q} &= \begin{pmatrix} \rho \\ \rho u \\ \rho v \\ e \end{pmatrix}, \quad \mathbf{F} = \begin{pmatrix} \rho u \\ \rho u^2 + p \\ \rho uv \\ (e + p)u \end{pmatrix}, \quad \mathbf{G} = \begin{pmatrix} \rho v \\ \rho uv \\ \rho v^2 + p \\ (e + p)v \end{pmatrix}, \\ \mathbf{F}^v &= \begin{pmatrix} 0 \\ \tau_{xx} \\ \tau_{xy} \\ u\tau_{xx} + v\tau_{xy} + \kappa \frac{\partial T}{\partial x} \end{pmatrix}, \quad \mathbf{G}^v = \begin{pmatrix} 0 \\ \tau_{xy} \\ \tau_{yy} \\ u\tau_{xy} + v\tau_{yy} + \kappa \frac{\partial T}{\partial y} \end{pmatrix}, \\ \tau_{xx} &= \mu \left(\frac{4}{3} \frac{\partial u}{\partial x} - \frac{2}{3} \frac{\partial v}{\partial y} \right), \quad \tau_{xy} = \mu \left(\frac{\partial u}{\partial y} + \frac{\partial v}{\partial x} \right), \quad \tau_{yy} = \mu \left(\frac{4}{3} \frac{\partial v}{\partial y} - \frac{2}{3} \frac{\partial u}{\partial x} \right). \end{aligned} \right\} \quad (2)$$

The system is closed by the equation of state of a perfect gas,

$$p = \rho T / \gamma. \quad (3)$$

In (1)–(3), u and v are the x and y components of the velocity vector; p is the pressure; ρ is the density; T is the temperature; $e = p/(\gamma - 1) + \rho(u^2 + v^2)/2$ is the total energy per unit volume; γ is the ratio of specific heats; μ is the dynamic coefficient of viscosity; and $\kappa = \mu/((\gamma - 1)Pr)$ is the coefficient of thermal conductivity. The viscosity is calculated with the Sutherland formula $\mu = T^{1.5}(1 + T_S/T_\infty)/(T + T_S/T_\infty)$, where T_∞ is the free-stream temperature and T_S is the Sutherland constant equal to 106.67 K for nitrogen. The Reynolds number Re_L is based on the free-stream parameters and the plate length L , and the Prandtl number is $Pr = 0.72$.

For (2) and (3) to be written in dimensionless form, the density, temperature and viscosity are normalized to their free-stream values; the other scaling quantities are the velocity of sound c_∞ for velocity, $\rho_\infty c_\infty^2$ for pressure and the plate length L for geometric sizes.

The numerical method used to solve (1) was described in detail in Kudryavtsev *et al.* (2006). The convective terms of the Navier–Stokes equations are approximated by the monotonicity-preserving, fifth-order (MP5) scheme proposed by Suresh & Huynh (1997). The fluxes through the faces between the cells are calculated by means of fourth-order piecewise-polynomial reconstruction; as a result, the scheme ensures fifth-order approximation on smooth solutions. Near the discontinuities, the reconstructed values of the fluxes are limited for the solution to preserve its monotonicity. This scheme has a built-in analyser distinguishing solution discontinuities from smooth extrema, which allows avoiding the decrease in accuracy on smooth extrema to the first order.

Flux reconstruction is performed in local characteristic variables; before reconstruction, the characteristic fluxes are split into positive and negative parts. The global Lax–Friedrichs splitting (Shu & Osher 1989) is used for this purpose in the present work. The diffusive terms in (1) are approximated with the fourth order of accuracy; both central and skewed differences are used to preserve a rather compact stencil (five cells in each direction) (Kudryavtsev & Khotyanovsky 2005). Integration in time is performed by the third-order total-variation-diminishing Runge–Kutta scheme (Shu & Osher 1988).

The code based on this numerical scheme was intensively tested and verified by comparing numerical results with well-known analytical solutions of compressible Navier–Stokes equations. In particular, the problems of the interior structure of the shock wave, the laminar supersonic boundary layer on the flat plate (at high Reynolds numbers, when the leading-edge shock wave is very weak, the boundary layer is thin, and the solution of the Navier–Stokes equations can be compared favourably with the self-similar solution of the boundary-layer equations) and viscous attenuation of a small-amplitude acoustic wave propagating in a uniform supersonic stream were solved. The two last test cases are directly connected with the problem under consideration.

When simulating processes in the hypersonic viscous shock layer, the following computational domain and the boundary conditions are taken. A schematic of the computational domain is shown in figure 9. The domain is a rectangle with sizes $L_x L_y$. The largest part EF of its lower side AD coincides with the plate surface, so that the streamwise size of the computational domain is $L_x = 1.05L$, where L is the plate length. The left (inflow) boundary AB is located at a distance of eight computational cells upstream from the leading edge of the plate (point E). The height

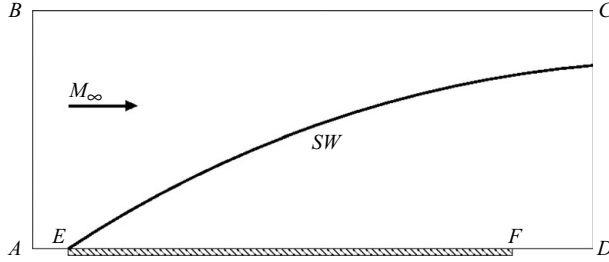


FIGURE 9. Schematic of the computational domain.

of the computational domain $L_y = 0.24L$ is chosen under the condition that the bow shock wave SW emanating from the leading edge does not interact with the upper boundary BC . Concerning the flow characteristic scales, the boundary-layer thickness δ in the cross-section $x = 0.8$ is $0.11L$, whereas the distance between the plate surface and the shock wave is $0.15L$. The definition of δ here is based on the streamwise velocity equal to 0.99 of that directly behind the shock wave, and the cross-section $x = 0.8$ is chosen because the boundary layer there is not yet subjected to the upstream influence of the wake flow behind the plate trailing edge. The right (outflow) boundary CD is separated from the trailing edge of the plate (point F) by the distance $0.042L$, which is sufficient for the flow in the exit section to be completely supersonic.

A uniform computational grid consists of $N_x = 1050$ cells in the streamwise direction and $N_y = 240$ cells in the transverse direction. All numerical data presented below are obtained for $M_\infty = 21$, $Re_L = 1.44 \times 10^5$ and a fixed surface temperature $T_w = 300$ K.

4. Steady flow

The steady basic flow is first calculated with a uniform hypersonic flow being imposed on the left (AB) and upper (BC) boundaries. The solution on the right boundary CD is extrapolated from inside the computational domain. The boundary conditions on the plate (EF) take into account the velocity slip and the temperature jump:

$$u = \frac{2 - a_u \alpha_u}{\alpha_u} \lambda \frac{\partial u}{\partial y}, \quad T - T_w = \frac{2 - a_e \alpha_e}{2\alpha_e} \frac{\gamma}{\gamma - 1} \frac{\lambda}{Pr} \frac{\partial T}{\partial y} \quad \text{for } y = 0, 0 < x < L. \quad (4)$$

Here $\lambda = \sqrt{\pi/2} \mu / \sqrt{p\rho}$ is the mean free path of molecules; α_u and α_e are the momentum and energy accommodation coefficients assumed to be equal to unity in the computations; and $a_u = 0.858$ and $a_e = 0.827$ are numerical coefficients whose values are obtained from an approximate solution of the Boltzmann equation in the Knudsen layer (Kogan 1969). The boundary conditions on the flat plate are supplemented with the non-permeability condition $v = 0$ for the vertical component of velocity and by the condition $\partial p / \partial y = 0$ for pressure. The conditions of symmetry are set on the remaining parts of the lower boundary (AE and DF). Numerical implementation of the boundary conditions involves ghost cells outside the computational domain.

The computed mean flow was compared with experimental data. Figure 10(a–c) shows the computed (solid curves) and experimental (symbols) profiles of the mean density in the cross-sections $x = 0.23$, 0.31 and 0.65 . The computed and experimental distributions of the Mach number in the same cross-sections are plotted in figure 10(d–f). The dashed curves in the figure show the profiles obtained by solving the Navier–Stokes equations with the no-slip boundary conditions.

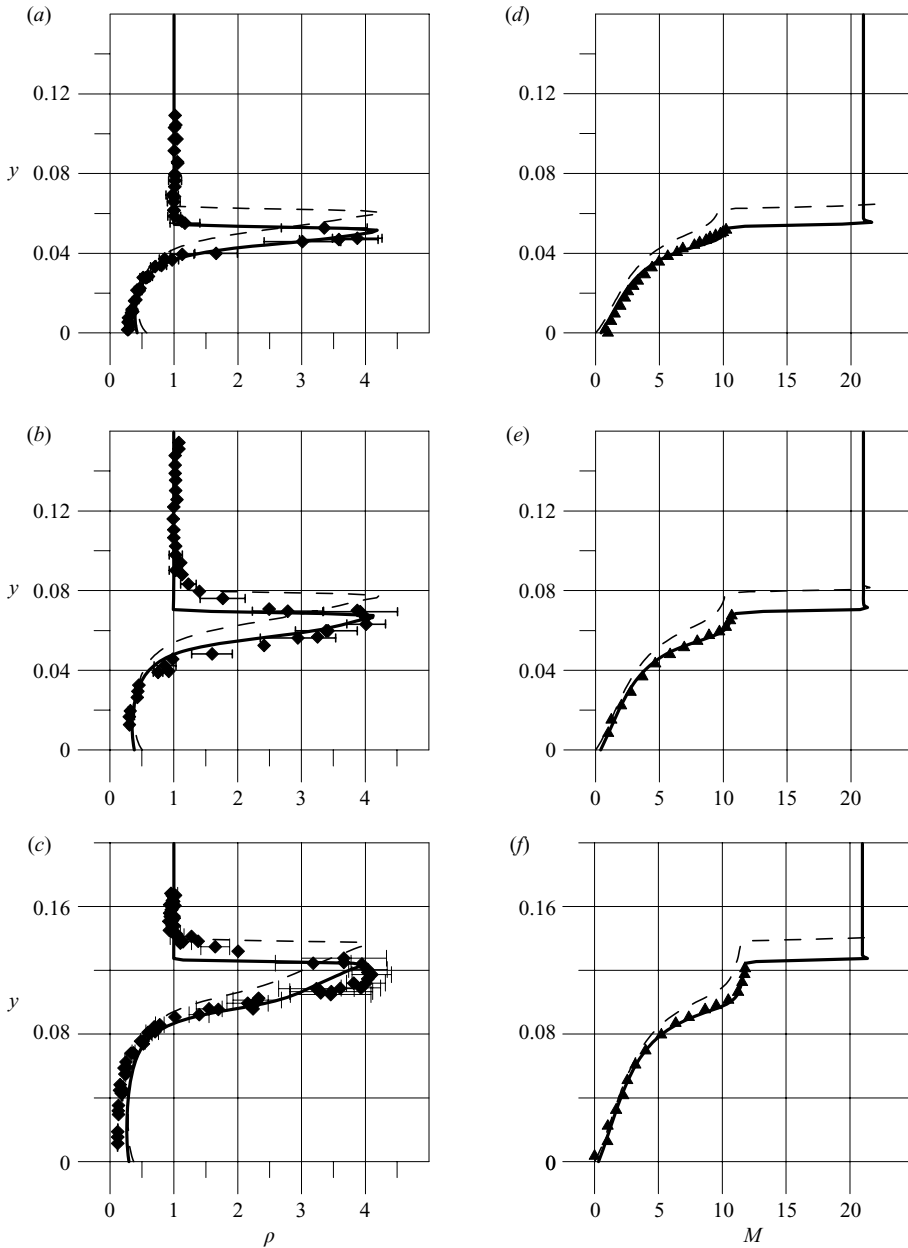


FIGURE 10. Density and Mach numbers profiles in the cross-sections $x = (a, d) 0.23$, $(b, e) 0.31$ and $(c, f) 0.65$ for steady flow: the dashed curves show the numerical data with the no-slip boundary conditions; the solid curves are the numerical data with the velocity slip and the temperature jump on the plate surface; the symbols are the experimental data.

The rarefaction effects are seen to be quite significant in this problem. The streamwise velocity on the plate surface is approximately 17% of its free-stream value at $x = 0.1$ and 7% near the trailing edge. It is evident from figure 10 that the allowance for the slip velocity and temperature jump on the plate surface noticeably improves the agreement with the experimental results. We can conclude that the

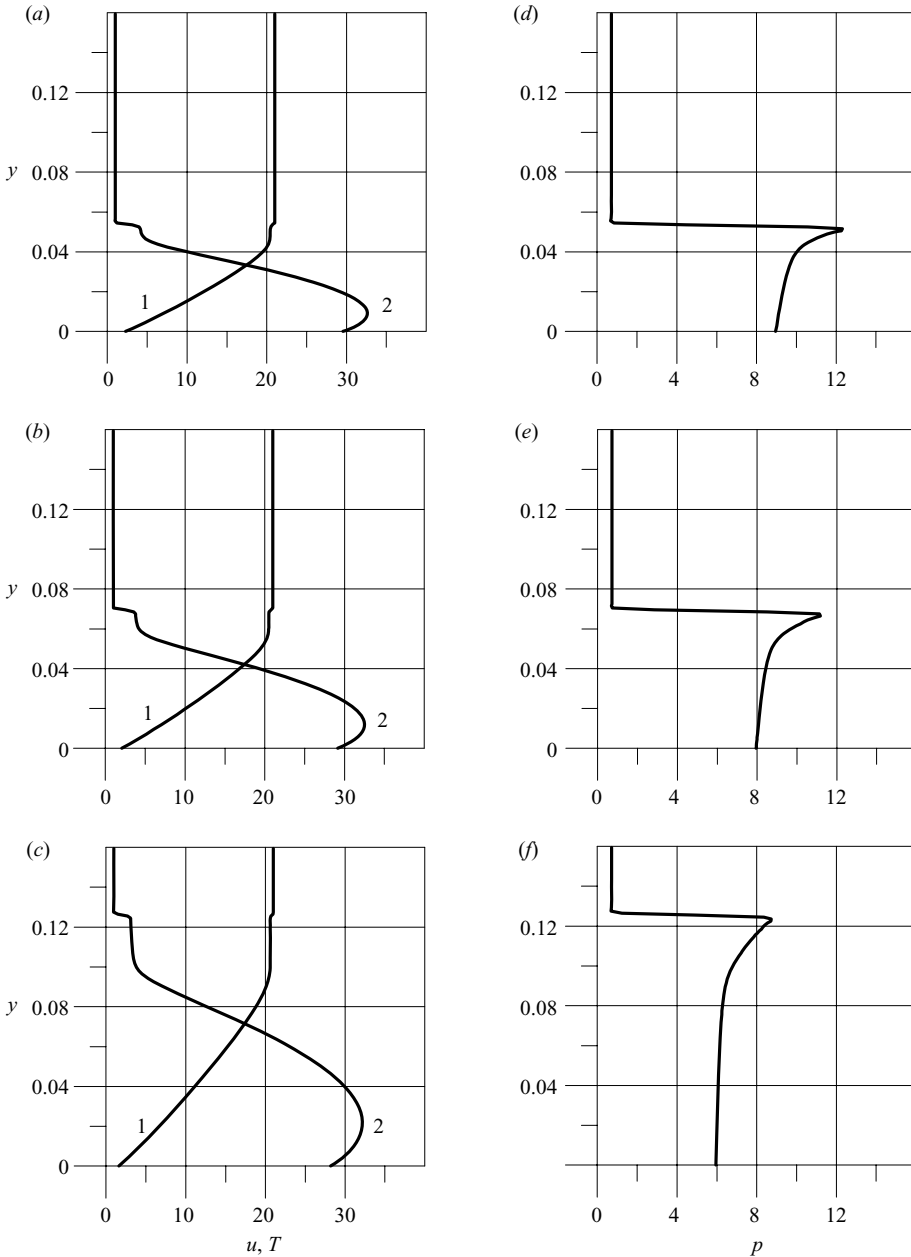


FIGURE 11. Mean velocity (denoted by 1), temperature (denoted by 2) and pressure profiles in the cross-sections $x = (a, d) 0.23$, $(b, e) 0.31$ and $(c, f) 0.65$ for steady flow (numerical data with the velocity slip and the temperature jump on the plate surface).

overall agreement between the computed and measured results is good. A certain difference in data for the mean density is caused by the substantial widening of the probing electron beam because of electron–molecule collisions in high-density regions and by smoothing of the real density profile.

The steady flow velocity, temperature and pressure profiles in several cross-sections are shown in figure 11. It can be seen that the temperature in the shock layer does

not exceed 400 K, and the pressure is substantially non-constant in the inviscid region of the shock layer.

5. Disturbances

In simulating the interaction of the viscous shock layer with natural and artificial disturbances, they are introduced by imposing appropriate time-dependent boundary conditions.

The natural disturbances observed in the experiments consist of acoustic waves propagating in the external flow. In numerical simulations of these disturbances, the variables on the left boundary of the computational domain (AD in figure 9) are set as a superposition of the steady basic flow and a plane monochromatic acoustic wave in the form

$$\begin{pmatrix} u' \\ v' \\ p' \\ \rho' \end{pmatrix} = A \begin{pmatrix} \pm \cos \theta \\ \mp \sin \theta \\ 1 \\ 1 \end{pmatrix} \exp[i(k_x x + k_y y - \omega t)]. \quad (5)$$

Here θ is the angle of propagation of the external acoustic wave; A is its amplitude; and $k_x = k \cos \theta$ and $k_y = -k \sin \theta$ are the components of the wave vector related to the angular frequency $\omega = 2\pi f$ by the dispersion relation $k = \omega / (M_\infty \cos \theta \pm 1)$. Here and in (5), the upper (lower) sign refers to the fast (slow) acoustic wave.

The boundary conditions on the plate surface are the same as those used to find the steady-state solution, except for the assumption of zero perturbations of temperature on the surface $T'|_{y=0} = 0$ (by virtue of a significant thermal inertia of the plate). Thus, the wall temperature is always equal to the temperature obtained in solving the steady-state problem. After introduction of disturbances, the Navier–Stokes equations are integrated until the unsteady solution reaches a periodic regime.

The artificial perturbations introduced in the experiments by the oblique-cut cylindrical whistle are perturbations similar to periodic blowing/suction organized locally, near the leading edge of the plate. In solving the problem numerically, they are simulated by setting the boundary condition for the transverse mass flow on a certain part of the plate surface:

$$\rho v|_{y=0} = A \sin\left(\pi \frac{x - x_1}{x_2 - x_1}\right) \sin \omega t. \quad (6)$$

Here, again, A is the amplitude and $x_1 = 0.065$ and $x_2 = 0.08$ are the boundaries of the region in which the perturbation was introduced. Except for that, the computation is performed in the same manner as the computation for acoustic perturbations.

6. Excitation of the shock layer by external acoustic disturbances

6.1. Spatial distribution of disturbances

Figure 12 shows the mean density flow field (figure 11a) and the instantaneous fields of density fluctuations for the case of excitation of the viscous shock layer by slow (figure 12b) and fast (figure 12c) acoustic perturbations of the external flow. The solid and dashed curves in figure 12(b, c) correspond to the positive and negative density fluctuations, respectively. It is seen from the figure that the main wave processes induced by external acoustic perturbations in the hypersonic shock layer occur behind the shock wave and on the edge of the hypersonic boundary layer. As

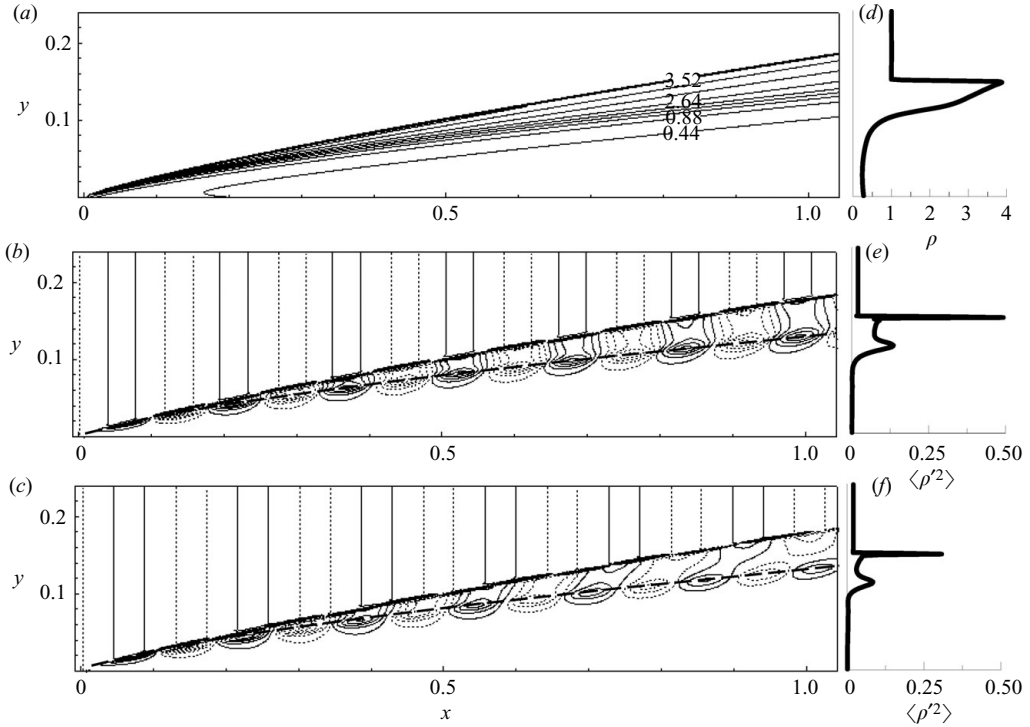


FIGURE 12. (a) Density isolines in steady flow, (b, c) isolines of instantaneous density fluctuations and r.m.s. fluctuations of density in the cross-section $x = (d, e, f)$ 0.8 with $\theta = 0^\circ$, $A = 0.028$ and $f = 38.4$ kHz: (b, e) fluctuations induced by a slow acoustic wave; (c, f) fluctuations induced by a fast acoustic wave; the dashed curve shows the position of the boundary-layer edge.

above, the boundary-layer edge is defined as the point at which the streamwise velocity is 1% smaller than the streamwise velocity immediately behind the shock wave. It is worth noting that this point coincides with the location of maximum gradient of mean density. The fluctuating characteristics of the flow in the hypersonic shock layer display a typical form with two maxima; the greater of them is located on the shock wave, and the position of the second maximum coincides with the boundary-layer edge (figure 12). This is seen in the figures of both the instantaneous isolines of density fluctuations (figure 12b, c) and the distributions of the root-mean-square (r.m.s.) fluctuations (figure 12e, f).

In the case of the external fast acoustic mode (figure 12c), the disturbances directly behind the shock wave leave behind the disturbances on the boundary-layer edge. This is not observed in the case of external slow acoustic waves (figure 12b). The reason is that the velocity of propagation of disturbances directly behind the shock wave is equal to the external flow velocity plus or minus the velocity of sound, depending on the mode of external acoustic disturbances. At the same time, the velocity of disturbances on the boundary-layer edge corresponds to the flow velocity there. In the case of the slow mode of external disturbances, the velocity on the boundary-layer edge is close to the external flow velocity minus the velocity of sound, while the velocity on the boundary-layer edge in the case of the fast mode is substantially

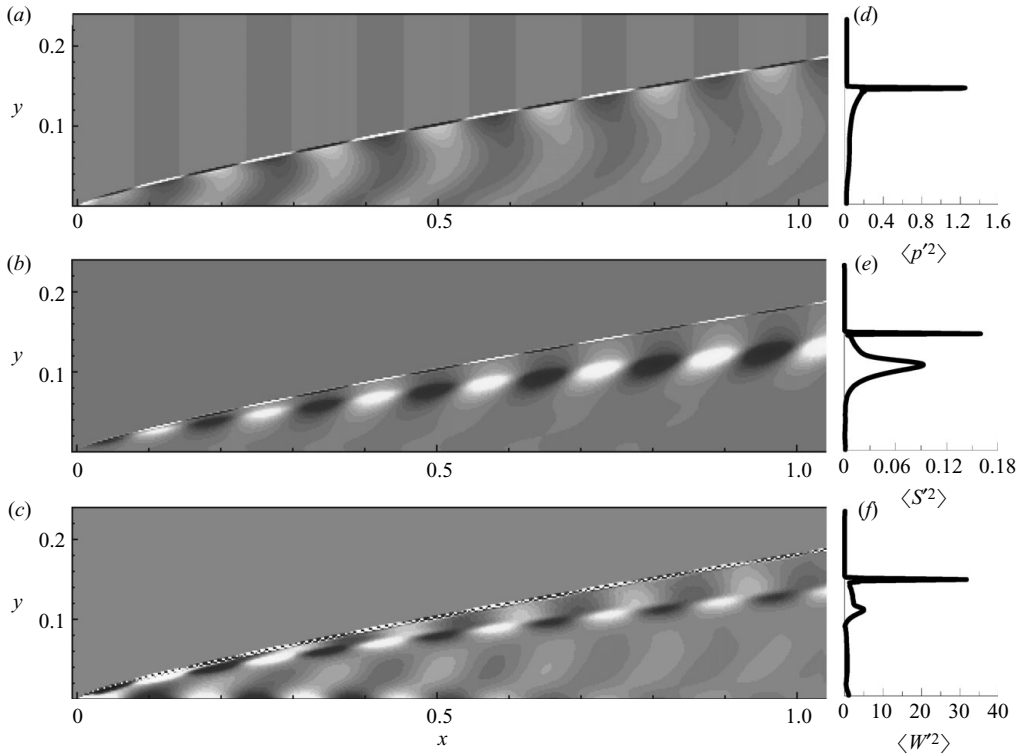


FIGURE 13. Instantaneous patterns of (a) pressure fluctuations in the shock layer, (b) entropy fluctuations and (c) vorticity fluctuations induced by a slow acoustic wave with $\theta = 0^\circ$, $A = 0.028$ and $f = 38.4$ kHz and r.m.s. profiles of (d) pressure, (e) entropy and (f) vorticity fluctuations in the cross-section $x = 0.8$.

smaller than the external flow velocity plus the velocity of sound, which leads to the observed phase delay.

Figure 13(a–c) shows the fields of pressure, entropy and vorticity fluctuations, respectively. A periodic structure of the fields is clearly visible. Vortices observed in figure 13(c) near the surface decay further downstream. Two maxima of fluctuations, on the shock wave and on the boundary-layer edge, are again observed in figure 13(b, c, e, f), while they are absent in the field of pressure fluctuations (figure 13a, d). Moreover, it is seen that the pressure fluctuations decay when moving from the shock wave inward into the shock layer.

Figure 14(a, b) shows a cut of the field of density fluctuations and the vector field of velocity fluctuations, respectively. It is seen that the shock layer contains vortices rotating in the opposite directions, which occupy the region between the shock wave and the boundary-layer edge. It is also seen that the light and dark regions of the field of density fluctuations correspond to the regions with velocity vectors directed towards and outward from the plate, respectively.

Thus, as a result of interaction of external acoustic waves with the hypersonic shock layer, vortex and entropy pulsations are generated, which propagate in the domain between the shock wave and the boundary-layer edge. At the same time, pressure fluctuations decay. It should be noted that such prevailing of the entropy–vortex mode is not typical for the boundary layer at moderate hypersonic Mach numbers, where

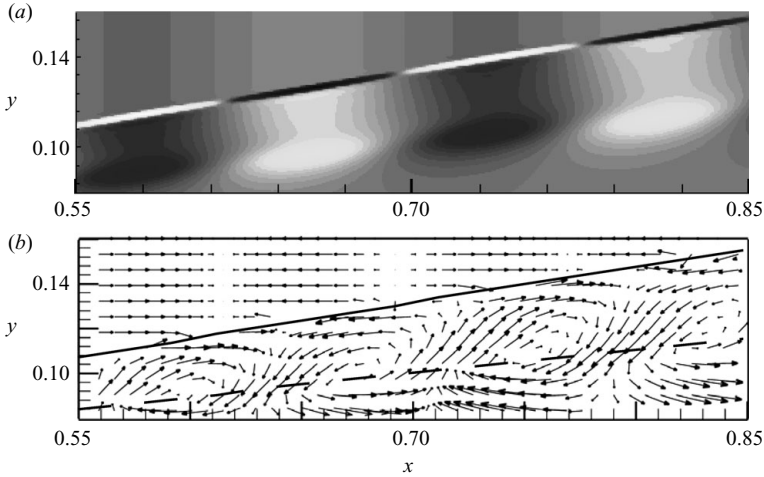


FIGURE 14. Instantaneous pattern of (a) density fluctuations in the shock layer and (b) vector field of velocity fluctuations induced by a slow acoustic wave with $\theta = 0^\circ$, $A = 0.028$ and $f = 38.4$ kHz: the solid and dashed curves show the locations of the shock wave and the boundary-layer edge, respectively.

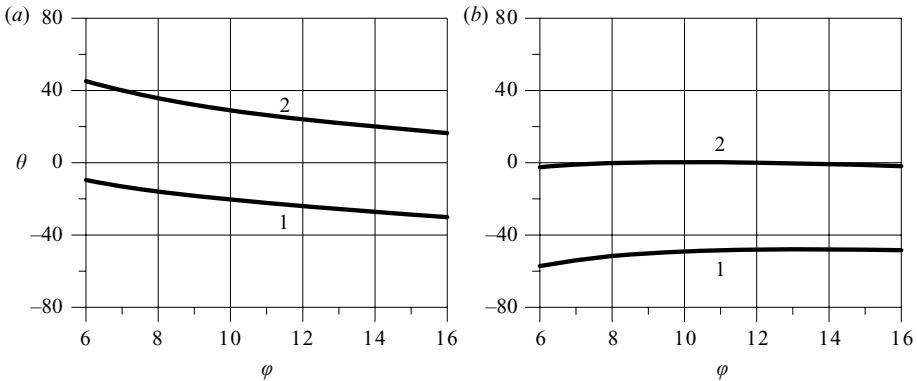


FIGURE 15. Critical angles for (a) slow and (b) fast incident acoustic waves at $M_\infty = 21$ versus the angle of shock wave inclination. Curves 1 and 2 bound the domain where no transmitted acoustic wave is generated.

the acoustic mode of instability is mainly developed (Egorov, Sudakov & Fedorov 2006a, b).

6.2. Comparison with the linear theory of interaction of small perturbations with a shock wave

It is known that all disturbances in a compressible fluid can be classified into acoustic, vortex and entropy modes. Acoustic disturbances propagate with the velocity of sound with respect to the flow, while vortex and entropy disturbances move along the streamlines together with the flow. Vortex and entropy waves can be considered as one mode of disturbances because they have the same dispersion relation, i.e. the entropy–vortex mode.

Figure 15 shows the regions of existence of perturbations of different modes in the shock layer, which were calculated in accordance with Kontorovich (1959)

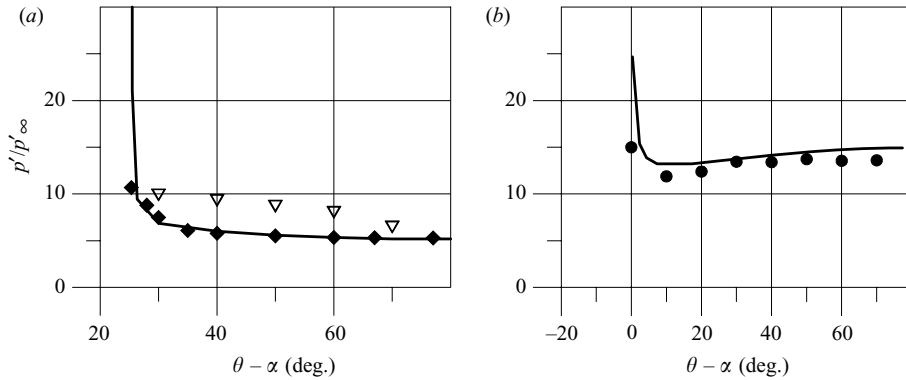


FIGURE 16. Transmission coefficient of pressure fluctuations behind the shock wave for external (a) slow and (b) fast modes: solid curve, theory of McKenzie & Westphal (1968); \blacklozenge and \bullet , numerical data for the inviscid case; ∇ , numerical data for the viscous case; $A = 0.028$ and $f = 80$ kHz.

and McKenzie & Westphal (1968). In accordance with the linear theory, there are the so-called critical angles bounding the range of propagation angles, where incident acoustic waves do not pass through the shock wave. In this range, the acoustic disturbances generated behind the shock wave exponentially decay further downstream. As was shown by measurements and computations, the shock wave inclination angle φ in the case considered changed from 16° near the leading edge of the plate to 7.5° at the end of the plate. Then, according to the linear theory of interaction of perturbations with the shock wave, the slow and fast external acoustic waves generate no transmitted acoustic waves in the domains of propagation angles between curve 1 and curve 2 (figure 15). Thus, only the entropy–vortex disturbances are generated inside the range of θ bounded by curves 1 and 2.

The analytical theory of interaction (Kontorovich 1959; McKenzie & Westphal 1968) was developed for inviscid flows. For comparisons with the theory, an inviscid hypersonic flow with $M_\infty = 21$ past a flat plate at a 10° angle of attack was computed by the method described above. This angle of attack was chosen to obtain the shock wave inclination angle φ close to that in the problem of a viscous flow past a flat plate at a zero angle of attack ($\varphi = 12.65^\circ$ in the cross-section $x = 0.2$).

The acoustic wave transmission coefficients, i.e. the ratios of the amplitudes of pressure fluctuations in the transmitted acoustic waves p' to the amplitudes of free-stream pressure fluctuations p'_∞ , were calculated. Figure 16(a, b) shows a comparison between the numerical transmission coefficients (symbols) and the data obtained on the basis of the linear theory of interaction (solid curves) for slow and fast acoustic waves, respectively, in the range of the propagation angles θ greater than the critical value (curve 2 in figure 15). The range of smaller angles is not considered because the transmitted acoustic waves decay exponentially with the distance from the shock wave in this case. The transmission coefficient of acoustic waves in the inviscid case is determined from the amplitude of pressure fluctuations on the surface with allowance for single reflection of disturbances from the plate surface and the shock wave.

It is seen from figure 16 that the acoustic waves are amplified manifold when passing through the shock wave. Thus, the amplification rate equals 5 in the case of incidence of a slow acoustic wave and is more than 13 in the case of incidence of a fast acoustic wave. For angles θ close to the critical angle of incidence, the theory

predicts a drastic increase in the amplification rate of acoustic waves (as $M_\infty \rightarrow \infty$, the amplification rate is proportional to M_∞^2 at the normal incidence and to M_∞^3 in the case of incidence at the critical angle). Such a drastic increase was not observed in the present computations. This agrees with the data of Zang, Hussaini & Bushnell (1984) and Manesh *et al.* (1995), where similar results were obtained in numerical simulations of interaction of acoustic disturbances with the normal shock wave.

Figure 16(a) also shows the amplification rates for the viscous case (triangles). They were computed as the ratio of the amplitude of pressure fluctuations directly behind the shock wave to the amplitude of free-stream pressure fluctuations at a distance x corresponding to the shock wave inclination angle $\varphi = 12.65^\circ$. This angle is close to the value of φ in the inviscid case. It seems that the observed differences of transformation coefficients for the viscous and inviscid cases are connected with generation, in the viscous case, of additional disturbances by a shear flow.

6.3. Mechanism of formation of the field of density fluctuations

The computed distributions of r.m.s. density fluctuations across the viscous shock layer are in good agreement with the measured results, which have a typical form with two maxima; the greater of them is located on the shock wave, and the position of the second maximum coincides with the boundary-layer edge (figure 17a).

The relation between the pulsations of density and those of normal velocity is demonstrated in §6.1. This suggests that density fluctuations are caused by mean flow field oscillations normal to the plate surface in the shock layer (see figure 14b), which are induced by vortices. Figure 17(b) shows the computed distributions of the mean density gradient (curve 1 is plotted only up to the shock wave because of the large gradient of mean density of the shock wave) and r.m.s. density fluctuations (curve 2) in the cross-section $x = 0.63$. The maxima of density fluctuations are seen to coincide with the maxima of the mean density gradient. Figure 17(b) also shows the distribution of density fluctuations (curve 3) obtained for small oscillations of the computed mean density profile along the normal to the surface. The amplitude of normal velocity fluctuations was assumed to be proportional to the mean normal velocity. Some difference in the location of the maxima of curves 2 and 3 (figure 17b) is caused by the difference between the actual (curve 5 in figure 17c) and the model distribution of normal velocity fluctuations. Nevertheless, curves 2 and 3 in figure 17(b) are in good agreement, which confirms the initial assumption that the field of density fluctuations is formed by normal-to-plate-surface oscillations of the mean density field in the shock layer, which are induced by vortices arising behind the shock wave under the action of external flow perturbations. This simple physical model also offers an explanation for the 180° phase shift between the fluctuations on the boundary-layer edge and the shock wave and for the large difference in their amplitude.

In addition, figure 17(d) shows the profiles of the mean streamwise velocity and its r.m.s. fluctuations in the same cross-section. The maxima of longitudinal velocity fluctuations do not coincide with those of density fluctuations. This confirms the above-described model of formation of the field of density fluctuations.

The solid curves in figure 18 show the behaviour of the computed amplitudes of density fluctuations immediately behind the shock wave for different frequencies of the slow (figure 18a) and fast (figure 18b) modes of external acoustic perturbations. The symbols in figure 16(a) are the measured amplitudes of density fluctuations at the corresponding frequencies. Good agreement between the computed and the experimental amplitude is observed within the accuracy of measurement. It is also seen in the figures that the distributions of the amplitudes of density fluctuations

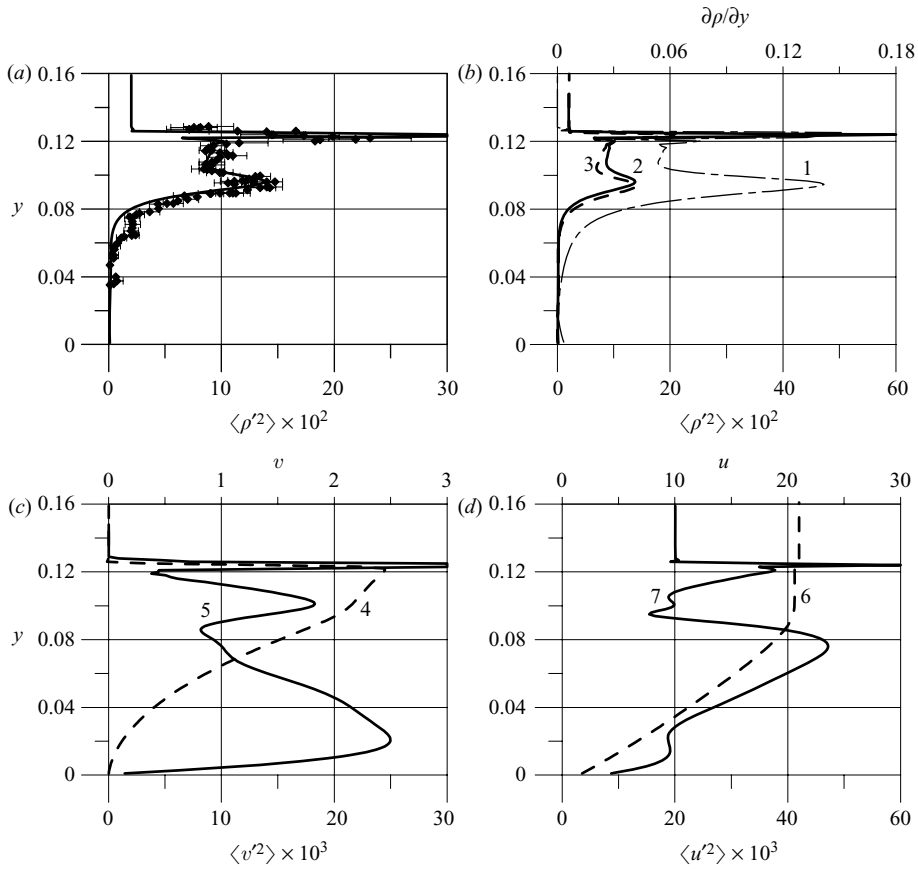


FIGURE 17. (a) Comparison of the computed profile of r.m.s. fluctuations of density (solid curve) with experimental data (\blacklozenge). (b) Computed distributions of the mean density gradient (denoted by 1), density fluctuations (denoted by 2) and density fluctuations predicted by the physical model (denoted by 3). (c) Computed distributions of the mean normal velocity (denoted by 4) and normal velocity fluctuations (denoted by 5). (d) Computed distributions of the mean longitudinal velocity (denoted by 6) and its fluctuations (denoted by 7). Slow acoustic wave $\theta = 0^\circ$, $A = 0.028$, $f = 38.4$ kHz, cross-section $x = 0.63$.

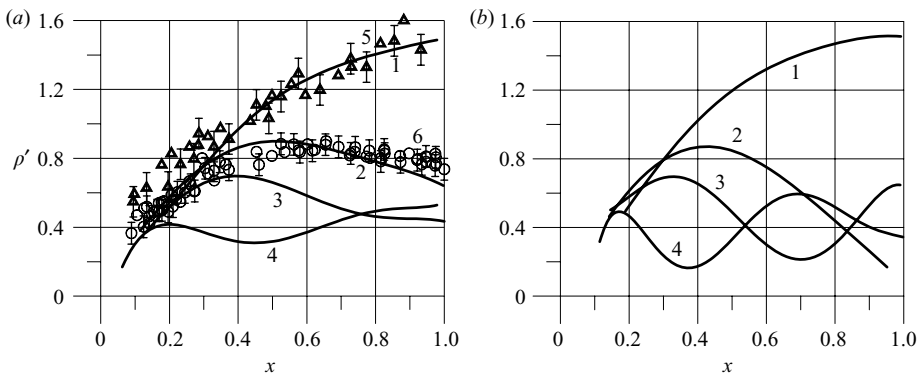


FIGURE 18. Amplitudes of density fluctuations directly behind the shock wave for (a) slow and (b) fast acoustic waves with $\theta = 0^\circ$ and $A = 0.028$ versus the streamwise coordinate for different frequencies: 1 and 5 denote 19.2 kHz; 2 and 6 denote 38.4 kHz; 3 denotes 50 kHz; and 4 denotes 80 kHz.

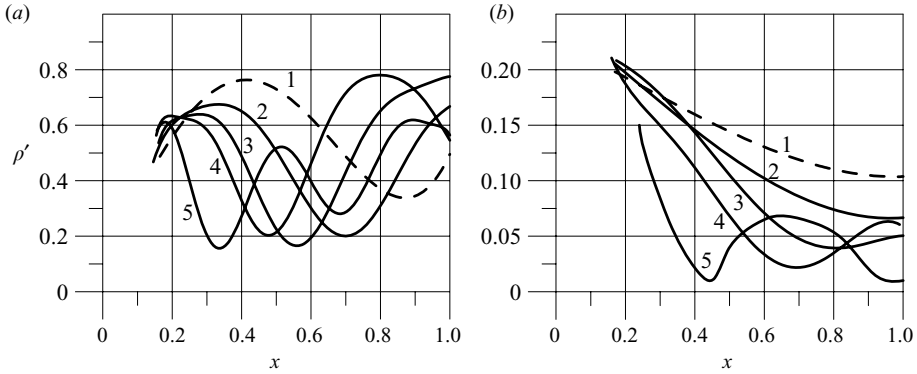


FIGURE 19. Amplitude of density fluctuations (a) directly behind the shock wave and (b) on the boundary-layer edge versus the streamwise coordinate for a fast acoustic wave with $A = 0.028$, $f = 50$ kHz and $\theta = -10^\circ, 0^\circ, 10^\circ, 20^\circ$ and 45° (denoted respectively by 1–5).

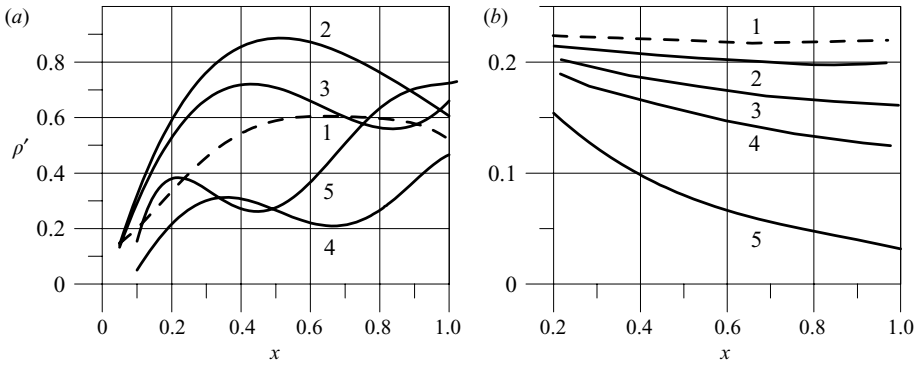


FIGURE 20. Amplitude of density fluctuations (a) directly behind the shock wave and (b) on the boundary-layer edge versus the streamwise coordinate for a slow acoustic wave with $A = 0.028$, $f = 38.4$ kHz and $\theta = -10^\circ, 0^\circ, 10^\circ, 20^\circ$ and 45° (denoted respectively by 1–5).

directly behind the shock wave as functions of the streamwise coordinate become non-monotonic with increasing frequency. At low frequencies (curves 1 and 2), only some part of the period of variations, which looks as a monotonic dependence on x , is recorded within the plate length. It seems that the distribution of density fluctuations is not monotonic at any frequency.

6.4. Influence of the propagation angle

Computations for different angles of propagation of external acoustic perturbations $\theta = -10^\circ, 0^\circ, 10^\circ, 20^\circ$ and 45° (figure 19a,b) with a frequency $f = 50$ kHz also revealed the presence of periodic variations of the amplitude of density fluctuations immediately behind the shock wave along the plate; the wavelength of these variations decreased with increasing frequency and angle of propagation of external acoustic perturbations. Variations of the amplitude of density fluctuations were also observed on the inner maximum (on the boundary-layer edge).

Similar dependencies of the amplitude of density fluctuations on the propagation angle are plotted in figure 20 for slow external acoustic waves. The dependencies obtained immediately behind the shock wave are non-monotonic.

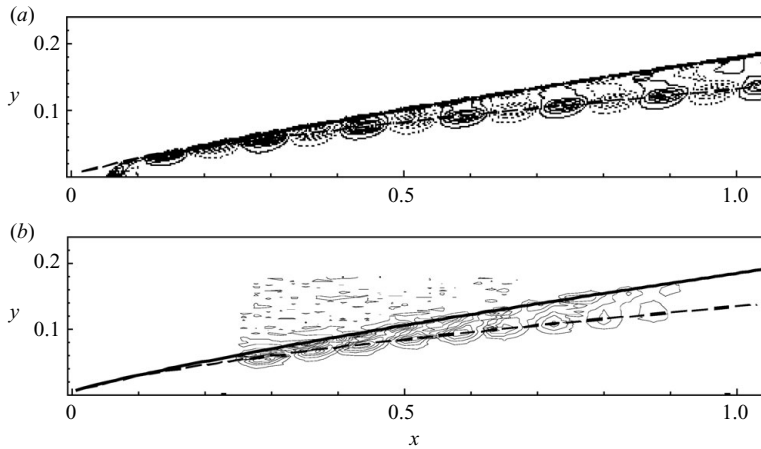


FIGURE 21. Instantaneous density fluctuations induced by periodic perturbations from the plate surface at a frequency $f = 40$ kHz: (a) numerical simulation, $A = 0.028$; (b) experiment; the solid and dashed curves show the locations of the shock wave and the boundary-layer edge, respectively.

It was initially assumed that these variations were caused by interference of external acoustic perturbations and vortex perturbations behind the shock wave, which had different phase velocities. The calculations for the external vortex mode, however, revealed the presence of amplitude variations with similar characteristics, though the phase velocities of external and internal perturbations in this case were almost identical. Hence, the characteristics of these variations are independent of or weakly depend on the mode of external perturbations.

An analysis of disturbances arising in the shock layer showed that both acoustic and vortex disturbances were generated behind the shock wave under the action of external perturbations of all modes. The field of density fluctuations in the shock layer was formed under the action of vortex and acoustic waves arising in the shock layer and propagating with different streamwise phase velocities. The mechanism of formation of the field of density fluctuations because of vortex disturbances was described above. Acoustic waves generated within the shock layer (which can be decaying or non-decaying, depending on the angle θ and the region of existence in figure 15) are directly responsible for density fluctuations in the shock layer. This simultaneous influence of two types of waves is manifested by variations of the amplitude of density fluctuations and can be interpreted as density wave interference accompanied by ‘beats’ of the amplitude of fluctuations. In the case of decaying acoustic waves behind the shock wave, variations of the amplitude of fluctuations are observed only behind the shock wave (figure 20a), where the maximum intensity of decaying acoustic waves is still high enough. In the case of non-decaying acoustic waves (at large angles of propagation of the external acoustic wave), variations of the amplitude of fluctuations are observed both directly behind the shock wave (figure 19a) and on the boundary-layer edge (figure 19b).

7. Excitation of the shock layer by disturbances introduced from the plate

Figure 21 shows the instantaneous density fluctuations in the shock layer on a flat plate, generated by a blowing/suction source at a frequency $f = 40$ kHz, which were

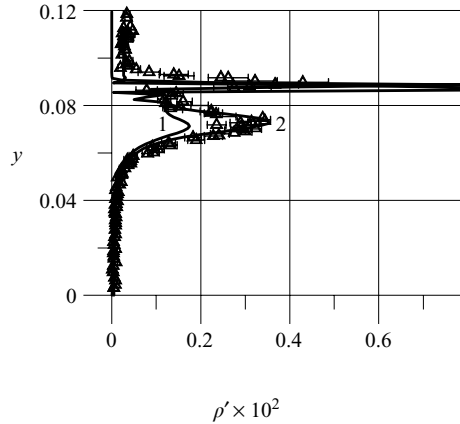


FIGURE 22. Profiles of density fluctuations across the shock layer, which are generated by a blowing/suction source ($f = 20$ kHz and $A = 0.028$), in the cross-section $x = 0.42$: curve 1 is the numerical data for an external slow acoustic wave (for comparison); the symbols and the solid curve, curve 2, show the experimental and computed results.

obtained (*a*) in DNSs and (*b*) in experiments with a whistle. It is seen that the field of intense fluctuations occupies the region between the shock wave and the boundary-layer edge, which corresponds to the maximum gradient of the mean density, as in the case of external acoustic perturbations. The computed data (figure 21*a*) agree with the experimental data (figure 21*b*). Again, there are two maxima of intensity of density fluctuations; one of them (higher peak) is located on the shock wave, and the second maximum (lower peak) is located on the boundary-layer edge; the phases of the fluctuations on the shock wave and on the boundary-layer edge are shifted by 180° . Thus, the fields of disturbances excited by periodic blowing/suction in the shock layer are similar to the fields of fluctuations excited by external acoustic waves.

It is also seen in figure 21 that the disturbances immediately behind the shock wave propagate slower than those on the boundary-layer edge, which results in some phase delay. A possible explanation is that the disturbances behind the shock wave are generated exclusively from below, and the observed delay is caused by the increase in distance between the boundary-layer edge and the shock wave.

The computed (solid curve 2) and measured (symbols) distributions of density fluctuations across the shock layer in the cross-section $x = 0.42$ are compared in figure 22 for the case of excitation by blowing/suction. A comparison of these data with the distribution of density fluctuations in the shock layer, which are generated by external acoustic waves (curve 1), shows that these profiles are also similar. This fact points to a common nature of formation of the field of density fluctuations through a mechanism that involves the action of vortex perturbations on the mean density field, which was described above.

Thus, the main feature of the mechanism of formation of the field of density fluctuations in the shock layer excited by both external acoustic perturbations and periodic blowing/suction is domination of entropy–vortex disturbances inside the shock layer.

The numerical and experimental density fluctuations in the shock layer for the case of periodic blowing/suction are compared in figure 23. The figure shows the computed streamwise distributions of the amplitude of density fluctuations immediately behind the shock wave (figure 23*a*) and on the boundary-layer edge (figure 23*b*) for the

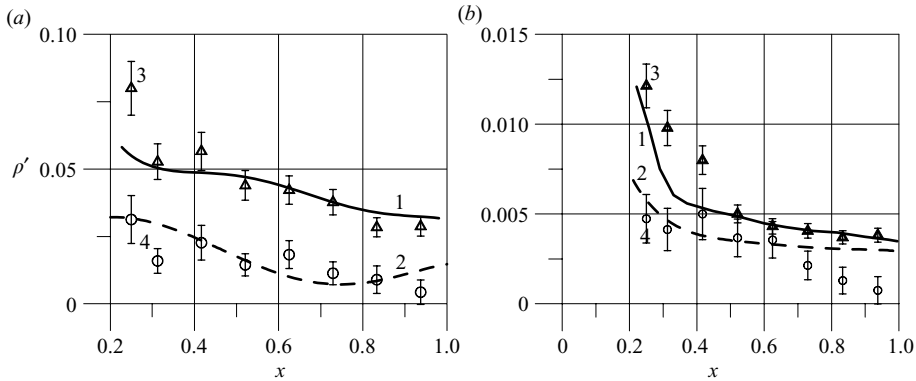


FIGURE 23. Comparison of experimental (symbols) and computed amplitudes of density fluctuations (a) directly behind the shock wave and (b) on the boundary-layer edge for frequencies of 20 kHz (1, 3, solid curve) and 40 kHz (2, 4, dashed curve) for blowing/suction perturbations with $A = 0.028$.

fundamental frequency $f = 20$ kHz and its harmonic $f = 40$ kHz. The symbols in the figures are the corresponding experimental data. Good agreement of experimental and computational results over a part of the plate (at $0.4 < x < 0.8$) is seen. Most probably, some difference between experimental and computed data over the initial part of the plate (at $x < 0.4$) is caused by different locations of the source of disturbances: in experiments, the disturbances are introduced by a whistle directly from the leading edge of the plate, while the perturbations in numerical simulations occur at a small distance from the leading edge. At $x > 0.8$, the influence of the plate trailing edge becomes substantial in experiments. A possible reason is flow three-dimensionality in the wake behind a flat plate of finite thickness and width, which was used in experiments.

A tendency of all density fluctuations to decay in the direction along the plate for the case with localized receptivity should be noted. This tendency can be caused by the fact that the influence of the perturbation source on the shock layer is gradually attenuated with distance from the source, while external perturbations affect the shock layer over its entire length.

The dependence of the magnitude of density fluctuations in the shock layer on the amplitude A of introduced perturbations was studied in the current work. Such information is important for controlling the intensity of fluctuations in the shock layer with the use of blowing/suction. Figure 24 shows the computed amplitude of density fluctuations as a function of the streamwise coordinate x (a) on the shock wave and (b) on the boundary-layer edge for three values of A , namely $A = 0.004$, 0.04 and 0.4 . A certain difference in the dependencies along the streamwise coordinate is seen in the figures. The most pronounced distortion of the distributions is observed in the region in which the blowing/suction source is placed. Nevertheless, the level of fluctuations in the shock layer increases almost linearly with increasing amplitude A of perturbations being introduced.

Figure 25 shows the amplitude of density fluctuations (a) on the shock wave and (b) on the boundary-layer edge as a function of the streamwise coordinate x at a frequency $f = 38.4$ kHz for three positions of the blowing/suction source. The distance from the source centre to the leading edge of the flat plate was $x = 0.0725$, 0.15 and 0.22 , and the amplitude of perturbations was $A = 0.04$. Obviously, the amplitude of

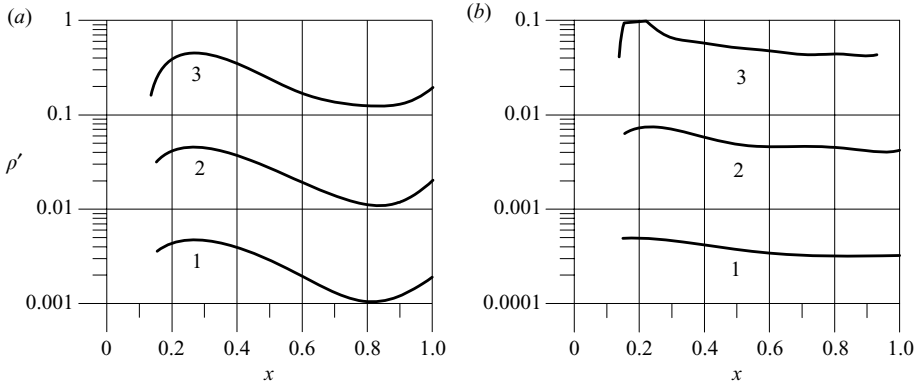


FIGURE 24. Amplitude of density fluctuations (a) directly behind the shock wave and (b) on the boundary-layer boundary versus the streamwise coordinate; $A=0.004$ (denoted by 1), 0.04 (denoted by 2) and 0.4 (denoted by 3); $f=38.4$ kHz.

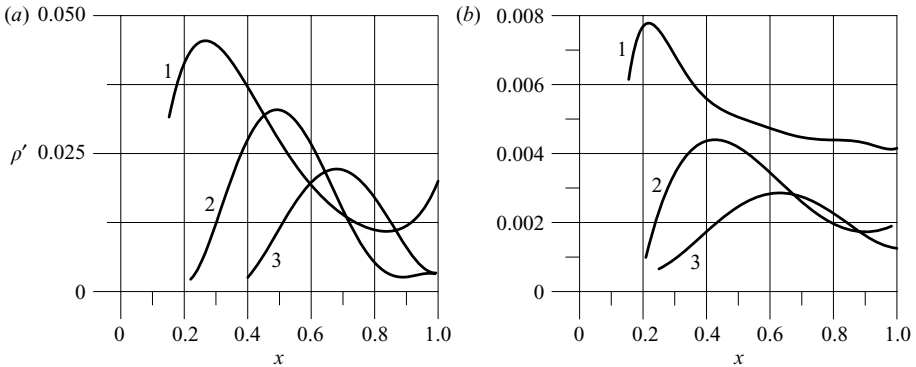


FIGURE 25. Amplitude of density fluctuations (a) directly behind the shock wave and (b) on the boundary-layer edge versus the streamwise coordinate for different positions of the blowing/suction source: $x=0.0725$ (denoted by 1), 0.15 (denoted by 2) and 0.22 (denoted by 3).

fluctuations in the shock layer decreases with increasing distance from the leading edge. It can be explained by the increase in the distance from the blowing/suction source to the high-density region behind the shock wave.

8. Active control of disturbances

It was demonstrated above that the entropy–vortex mode of disturbances dominates in the shock layer in the flow past a flat plate with a Mach number $M_\infty=21$ excited by both external acoustic perturbations and periodic blowing/suction. As a consequence, the spatial structures of disturbances under the action from outside and inside the shock layer are fairly similar (see figures 12 and 21). Figure 26 shows the streamwise phase velocity of disturbances C_x on the boundary-layer edge, normalized to the flow velocity behind the shock wave, as a function of the distance along the plate. The computations (solid and dashed curves in figure 26) and measurements (symbols) show that the streamwise phase velocities of disturbances generated both by external acoustic waves (triangles and circles) and by the source on the model

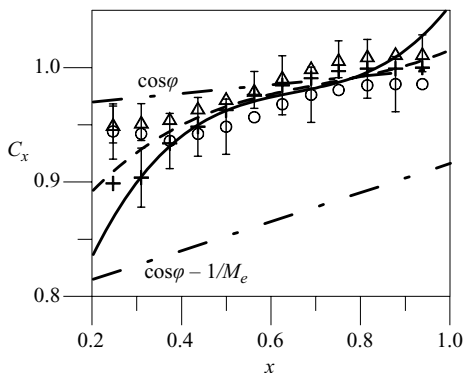


FIGURE 26. Streamwise phase velocity of disturbances on the boundary-layer edge versus the distance along the plate: measurements for fast and slow external acoustic waves (Δ and \circ); measurements for perturbations generated by the oblique-cut whistle (+); the solid and dashed curves show numerical results for fast and slow acoustic waves; the dash-dotted curves show the phase velocities of vortex and slow acoustic perturbations calculated using the linear theory of hydrodynamic stability.

surface (crosses) coincide. In addition, the phase velocity of vortex disturbances in the shock layer is close to the phase velocity of vortex disturbances (upper dash-dotted curve in figure 26) obtained within the framework of the locally parallel linear theory of stability (Gaponov & Maslov 1980) with allowance for the local shock wave inclination angle φ and local Mach number M_e . The lower dash-dotted curve in figure 26 shows the phase velocity of slow acoustic perturbations behind the shock wave.

Under these conditions, it is possible to use active methods of disturbance control, which work well in subsonic boundary layers (Biringen 1984; Nosenchuck 1988; Pack & Joslin 1998; Rist & Gmelin 2006). Oscillations generated by external perturbations can be suppressed by introducing artificial perturbations if an appropriate phase and amplitude of blowing/suction are selected.

8.1. Numerical simulations

In the present activities, the possibility of such control was demonstrated numerically and experimentally. Figure 27(a) shows the computed field of instantaneous density fluctuations in the shock layer on a flat plate excited by slow acoustic waves propagating at a zero angle to the external flow centreline. Hereinafter, for the sake of illustration, the field of isolines is supplemented with the r.m.s. (averaged over the period) dependence of density fluctuations on the normal coordinate y in the cross-section $x=0.8$ (figure 27e–h). These dependencies have a typical shape with two maxima; the higher maximum is located on the shock wave proper and is related to shock wave oscillations, and the location of the second maximum coincides with the boundary-layer edge. Figure 27(b) shows the field of instantaneous density fluctuations in the shock layer on a flat plate, which were generated by blowing/suction. Qualitative similarity of the fields of fluctuations and quantitative coincidence of the amplitude of density fluctuations on the boundary-layer edge are observed. Figure 27(c) shows the field of instantaneous density fluctuations in the shock layer on a flat plate under a joint action of external and internal sources of perturbations, when these sources operate exactly in the opposite phases. It is well

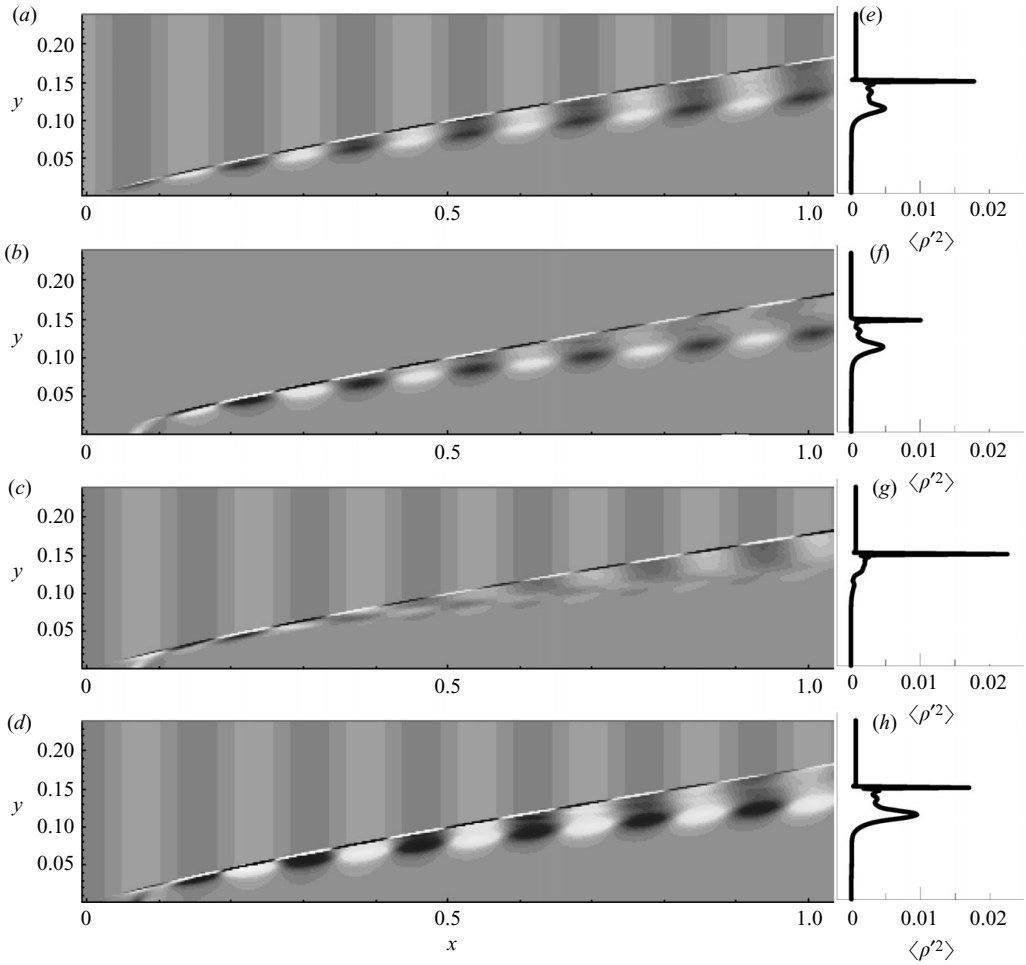


FIGURE 27. (*a–d*) Instantaneous density fluctuations in the shock layer and (*e–h*) r.m.s. density fluctuations in the cross-section $x=0.8$ for $\theta=0^\circ$ and $f=38.4$ kHz: (*a, e*) slow acoustic wave $A=0.001$; (*b, f*) blowing/suction from the plate surface $A=0.06$; (*c, g*) anti-phase action; (*d, h*) in-phase action.

seen that the density fluctuations on the boundary-layer edge decrease substantially, though the oscillations of the shock wave proper remain almost unchanged.

For the sake of illustration, figure 27(*d*) shows the field of instantaneous density fluctuations in the case of in-phase operation of the sources of perturbations. As was expected, the amplitude of fluctuations on the boundary-layer edge is doubled.

The maximum efficiency of suppression is achieved by selection of the blowing/suction amplitude and the time shift with respect to external acoustic disturbances. The values of the blowing/suction amplitude and the time shift depend on the type of external disturbances; therefore the transformation coefficients are different for slow and fast acoustic waves.

As is seen in figure 28, the phase control is equally efficient for both fast and slow external acoustic waves.

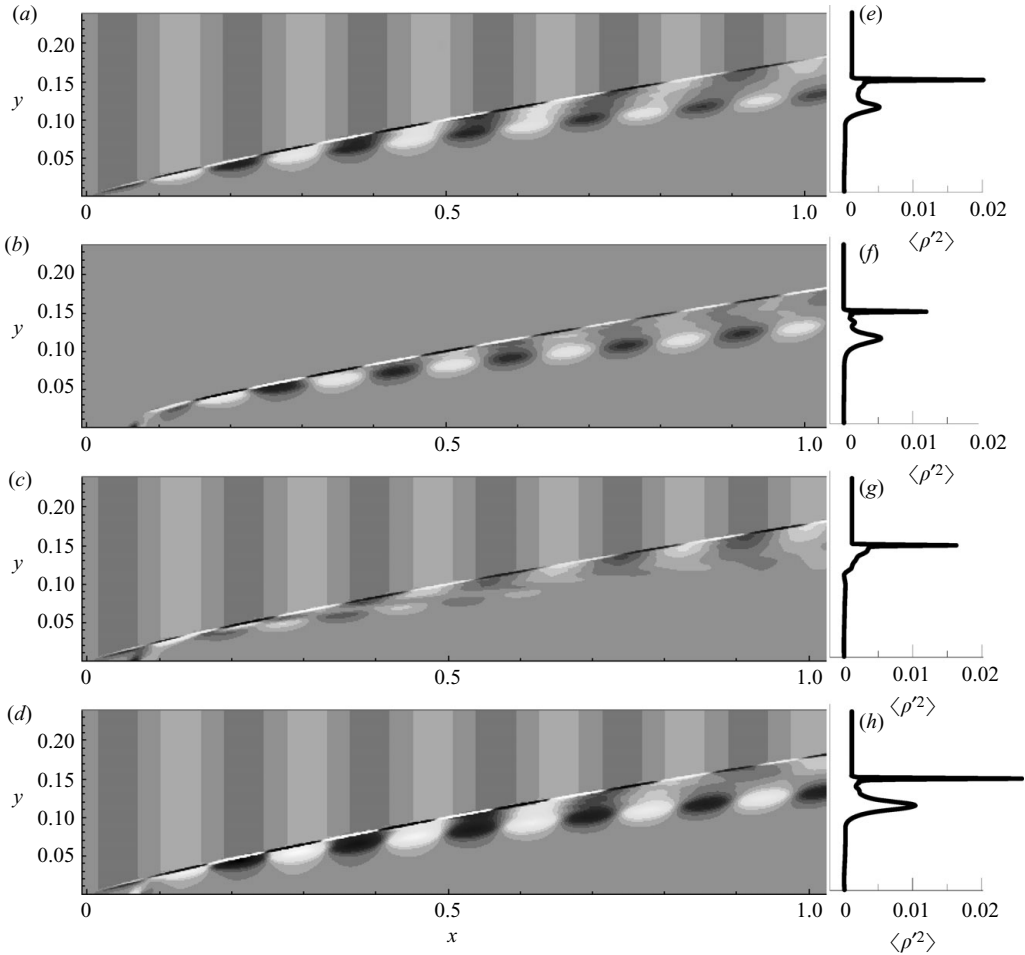


FIGURE 28. (a–d) Instantaneous density fluctuations in the shock layer and (e–h) r.m.s. density fluctuations in the cross-section $x = 0.8$ for $\theta = 0^\circ$ and $f = 38.4$ kHz: (a, e) fast acoustic wave $A = 0.0017$; (b, f) blowing/suction from the plate surface $A = 0.0694$; (c, g) anti-phase action; (d, h) in-phase action.

8.2. Experimental investigation

The results of numerical simulations were verified by experiments. The idea of the experiment is illustrated in figure 29. Periodic acoustic waves (1 in figure 29) are generated in a hypersonic flow. These waves interact with the shock layer on the plate (2 in figure 29) and generate fluctuations in the layer. The oblique-cut gas-dynamic whistle (3 in figure 29) located under the plate near the plate leading edge also introduces periodic pressure perturbations into the shock layer on the flat plate. If the frequency of external flow disturbances equals the frequency of perturbations introduced by the whistle, interference suppression (amplification) of fluctuations in the shock layer on the flat plate can occur under a certain relationship between the disturbance phases. For better understanding, the suppression of density fluctuations in the shock layer in figure 29 is shown at the time instant when the disturbances have passed half of the plate length after the whistle activation.

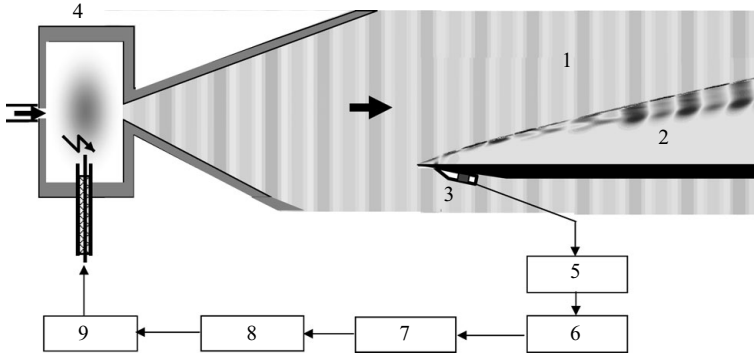


FIGURE 29. Arrangement of the experiment: 1, acoustic waves in the external flow; 2, flat plate; 3, oblique-cut whistle; 4, settling chamber; 5, amplifier; 6, narrow-band filter; 7, frequency divider; 8, generator of pulses for electric discharge initiation; 9, power unit for the discharge.

Acoustic perturbations (1 in figure 29) in the hypersonic free stream are generated by a powerful electric discharge in the settling chamber (4 in figure 29); a pulse synchronized with pressure oscillations in the resonator of the whistle (3 in figure 29) initiates the discharge. Thus, the phases of external and internal controlled periodic perturbations are correlated. The electric circuit used in the experiment is also shown schematically in figure 29. The circuit includes an amplifier of the signal of the transducer of pressure oscillations in the whistle (denoted by 5), a narrow-band filter for identifying the fundamental frequency of fluctuations (denoted by 6), a frequency divider (denoted by 7), a generator of pulses (denoted by 8) initiating the discharge with a possibility of a time shift with respect to the incoming signal and a power unit for the spark discharge (denoted by 9) with a controlled time of discharge initiation. In the experiment, the frequency of the transducer of pressure fluctuations in the whistle was divided by 5. The use of the frequency divider (7 in figure 29) made it possible to increase the power of an individual discharge pulse and to use the higher harmonics of pressure fluctuations in the settling chamber ($f_4 = 12.5$ kHz, $f_9 = 25$ kHz and $f_{14} = 37.5$ kHz) to form acoustic perturbations in the flow. The frequencies of these harmonics coincide with the fundamental frequency and also with the first and second harmonics of oscillations in the whistle. The amplitudes of density fluctuations generated in the shock layer by external acoustic waves and by the whistle at frequencies of 25 and 37.5 kHz were almost coincident. It was at these frequencies that the maximum effect of amplification was expected.

For three frequencies, $f = (a)$ 12.5, (b) 25 and (c) 37.5 kHz, figure 30 shows the experimental dependencies of the amplitude of density fluctuations on the boundary-layer edge on the flat plate $\langle \rho'^2 \rangle / \langle \rho'^2 \rangle_{max}$ in the cross-section $x = 0.63$ on the time shift $\Delta\tau$ between the external flow oscillations and oscillations generated by the oblique-cut whistle, which is normalized to the period of oscillations, T . Here $\langle \rho'^2 \rangle_{max}$ is the level of density fluctuations on the boundary-layer edge for the in-phase effect of the external acoustic wave and periodic disturbances of the blowing/suction type. The dependencies in figure 30 are plotted for different ranges of the quantity $\Delta\tau/T$. The reason is the normalization of the time shift to the period of oscillations at the corresponding frequencies.

The plots display periodic variations of the amplitude of density fluctuations. The depth of these variations depends on the ratio of the amplitudes of external acoustic and internal blowing/suction perturbations. At the fundamental frequency of the

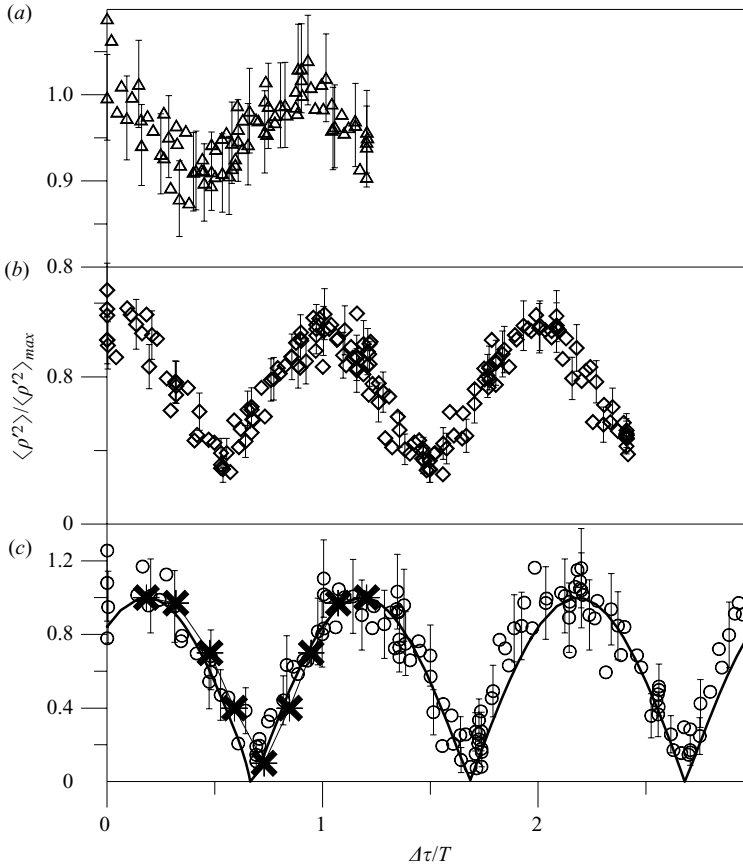


FIGURE 30. Normalized amplitudes of r.m.s. density fluctuations on the boundary-layer edge versus the delay between the whistle signal and discharge initiation for three frequencies: (a) 12.5, (b) 25 and (c) 37.5 kHz. The symbols are the measured data; the solid curve is the approximation by the dependence for interference of two sinusoidal waves of identical frequencies and amplitudes; the crosses are the numerical data.

whistle, the amplitude of perturbations introduced by the whistle is substantially greater than the amplitude of disturbances generated by external acoustic waves; therefore, no significant suppression of fluctuations occurs here. At the frequencies of the first and second harmonics, the ratio of the amplitudes of external and internal perturbations allows the fluctuations in the shock layer to be almost completely suppressed. Some displacement of the locations of minima and maxima with increasing frequency is caused by the phase shift of the discharge-controlling signal in the electronic circuit in figure 29.

For comparison, figure 30(c) shows the corresponding numerical data (crosses) in the shock layer under the action of fast acoustic waves propagating at a zero angle to the external flow centreline with a frequency $f = 37.5$ kHz and the dependence of amplitude in accordance with the law of interference of two harmonic waves of the same frequency and amplitude (solid curve).

The initial amplitudes of the fast external acoustic mode and periodic blowing/suction perturbations were chosen to fit the suppression problem: 0.0017

and 0.0694, respectively. The computed values are seen to be in good agreement with the measured data.

The measurements performed in several cross-sections in the range $x = 0.23\text{--}0.85$ show that the depth of modulation of the amplitude of oscillations and the value of $\Delta\tau/T$ that ensures the minimum (maximum) of density fluctuations remain unchanged. This fact indicates that suppression (amplification) of fluctuations occurs simultaneously over the entire plate length.

Variations of the amplitude of pulsations with the variation of $\Delta\tau/T$ are also observed immediately behind the shock wave; however, their permanent suppression or amplification in this region cannot be obtained because of a substantial difference in phase velocities of disturbances generated by external fast acoustic waves and the oblique-cut whistle (see figures 12*c* and 21*a*). Such suppression of fluctuations behind the shock wave is impossible to obtain with external acoustic disturbances of the slow mode because the phase velocity of fluctuations generated by these disturbances is larger than that of disturbances from the oblique-cut whistle.

9. Conclusions

A novel numerical and experimental investigation of generation and development of disturbances in a hypersonic shock layer on a flat plate at a zero angle of attack excited by external acoustic waves of the slow and fast modes, as well as by blowing/suction from a local source on the plate, is performed.

Experimental investigations are conducted in a hypersonic nitrogen-driven wind tunnel at a flow Mach number of 21 and Reynolds number of 1.44×10^5 . The mean density and Mach number distributions, as well as the characteristics of the field of density fluctuations in the free stream and in the shock layer, are measured by probing and electron-beam fluorescence techniques. In particular, the phase velocities and the propagation angles of free-stream disturbances, the r.m.s. and instantaneous amplitude distributions of fluctuations and their phase velocities in the shock layer are measured. The method of artificial wave packets is used in wind-tunnel experiments. Controlled periodic disturbances in the free stream are generated by an electric discharge or are introduced into the shock layer from the plate leading edge by an oblique-cut gas-dynamic whistle. Some part of the results is obtained with natural disturbances of the wind-tunnel flow.

Measurements of the wave characteristics of artificial and natural free-stream disturbances reveal their two-dimensional character, and the modal composition of these disturbances is determined. It is also shown that the oblique-cut whistle generates two-dimensional disturbances of the entropy–vortex mode in the shock layer.

DNSs of generation and development of disturbances in the shock layer during its interaction with fast and slow acoustic waves or with pulsations from a local source of blowing/suction on the plate surface are performed by solving the Navier–Stokes equations. A numerical parametric study is carried out, which includes the following: variations of the intensity and the angle of incidence of external disturbances on to the shock wave; the intensity of the blowing/suction source and its location on the plate; and the frequency of disturbances. New results on the transformation coefficients of external disturbances across the shock waves and the structure of fluctuations in the shock layer are obtained. Numerical results are in good agreement with wind-tunnel

measurements and predictions of the linear theory of interaction of disturbances with a shock wave.

It is demonstrated for the first time that external acoustic waves and pulsations forced by an oblique-cut whistle or a local source of blowing/suction on the plate surface predominantly generate disturbances of the entropy–vortex mode in the shock layer. Interacting with the mean flow, they form a specific flow field of density fluctuations. In particular, there are two maxima of density fluctuations: a narrow intense peak immediately behind the shock wave and a wider and less intense peak on the boundary-layer edge. Such a spatial distribution of fluctuations is typical for all types of shock-layer excitation being tested.

The phase velocity of disturbances on the boundary-layer edge coincides with the local gas velocity. The velocity of disturbance propagation behind the shock wave depends on the type of excitation. If the shock layer is excited by acoustic waves of the fast mode, then the disturbances immediately behind the shock wave propagate faster than those on the boundary-layer edge. In case of excitation by acoustic waves of the slow mode, the phase velocities of disturbances immediately behind the shock wave and on the boundary-layer edge are approximately identical. If the shock layer is excited by blowing/suction from the surface or by an oblique-cut whistle, the phase velocity of disturbances immediately behind the shock wave is lower than that on the boundary-layer edge.

A numerical parametric study of the influence of the propagation angle of external acoustic waves shows the existence of substantial streamwise variations of the amplitude of disturbances directly behind the shock wave and on the boundary-layer edge. The size of these variations depends on the propagation angle of external disturbances; their streamwise length scale is determined by both the propagation angle and the frequency of external disturbances. A possible explanation of the existence of amplitude variations is the interference of entropy–vortex disturbances in the shock layer with acoustic waves generated behind the shock wave. The properties of the streamwise variations depend on whether the acoustic waves generated behind the shock wave are decaying or propagating. The characteristics of decaying acoustic waves are described properly by the linear theory of interaction of perturbations with a shock wave.

The similarity of the fields of fluctuations generated in the shock layer by free-stream disturbances and by periodic blowing/suction, as well as the coincidence of the phase velocities of disturbances on the boundary-layer edge, allows the interference scheme to be used for controlling the intensity of fluctuations in the shock layer. This scheme enables one to control the intensity of fluctuations by means of artificial blowing/suction disturbances with a specified amplitude and phase. The interference scheme of flow control for flows with strong viscous–inviscid interaction is successfully implemented for the first time in both computations and experiments. Acoustic waves introduced into the incoming flow generate entropy–vortex disturbances in the shock layer. The latter are suppressed or amplified by disturbances generated by periodic blowing/suction (in numerical simulations) or by an oblique-cut whistle (in experiments). Almost complete extinction of fluctuations on the boundary-layer edge and appreciable suppression of fluctuations in the entire shock layer are obtained.

This work was supported by the Russian Foundation for Basic Research (projects 09-08-00557, 09-01-00524 and 09-08-00679) and by ADTP RNP 2.1.1/3963. The computer time for computations was allocated by the Siberian Supercomputer Centre.

REFERENCES

- ANISKIN, V. M. & MIRONOV, S. G. 2000 Experimental study of density fluctuations in a hypersonic jet in the wake behind a cone. *J. Appl. Mech. Tech. Phys.* **41** (3), 479–484.
- BECKWITH, I. E., HARVEY, W. D. & CLARK, F. L. 1971 Comparison of turbulent boundary layer measurements at Mach number 19.5 with theory and an assessment of probe errors. *Tech Note TN-D 6192*. NASA.
- BERTOLOTTI, F. P. & HERBERT, TH. 1991 Analysis of the linear stability of compressible boundary layers using the PSE. *Theoret. Comput. Fluid Dyn.* **3**, 117–124.
- BIRINGEN, S. 1984 Active control of transition by periodic suction-blowing. *Phys. Fluids* **27**, 1345–1355.
- BOIKO, A. V., GREK, G. R., DOVGAL, A. V. & KOZLOV V. V. 2002 *The Origin of Turbulence in Near-Wall Flows*. Springer.
- BORN, M. & WOLF, E. 1968 *Principles of Optics*. Pergamon.
- CHANG, C. L., MALIK, M. R., ERLEBACHER, G. & HUSSAINI, M. Y. 1991 Compressible stability of growing boundary layers using parabolized stability equations. *Paper 91-1636*. AIAA.
- CHANG, C. L., MALIK, M. R. & HUSSAINI, M. Y. 1990 Effects of shock on the stability of hypersonic boundary layers. *Paper 1990-1448*. AIAA.
- EGOROV, I. V., FEDOROV, A. V. & SUDAKOV, V. G. 2008 Receptivity of a hypersonic boundary layer over a flat plate with a porous coating. *J. Fluid Mech.* **601**, 165–187.
- EGOROV, I. V., SUDAKOV, V. G. & FEDOROV, A. V. 2004 Numerical modelling of perturbation propagation in a supersonic boundary layer. *Fluid Dyn.* **39** (6), 874–884.
- EGOROV, I. V., SUDAKOV, V. G. & FEDOROV, A. V. 2006a Numerical modelling of the receptivity of a supersonic boundary layer to acoustic disturbances. *Fluid Dyn.* **41** (1), 37–48.
- EGOROV, I. V., SUDAKOV, V. G. & FEDOROV, A. V. 2006b Numerical modelling of the stabilization of a supersonic flat-plate boundary layer by porous coating. *Fluid Dyn.* **41** (3), 356–365.
- FEDOROV, A., SHIPLYUK, A., MASLOV, A., BUROV, E. & MALMUTH, N. 2003 Stabilization of a hypersonic boundary layer using an ultrasonic absorptive coating. *J. Fluid Mech.* **479**, 99–130.
- FEDOROV, A. V., MALMUTH, N. D., RASHEED, A. & HORNUNG, H. G. 2001 Stabilization of hypersonic boundary layers by porous coatings. *AIAA J.* **39** (4), 605–610.
- FEDOROV, A. V. & TUMIN, A. 2004. Evolution of disturbances in entropy layer on blunted plate in supersonic flow. *AIAA J.* **42** (1), 89–94.
- FISHER, M. C., MADDALON, D. V., WEINSTEIN, L. M. & WAGNER, R. D., JR 1971 Boundary – layer Pitot and hot-wire surveys at $M_\infty \cong 20$. *AIAA J.* **9** (5), 826–834.
- FOMIN, V. M., KUDRYAVTSEV, A. N., MASLOV, A. A., MIRONOV, S. G., POPLAVSKAYA, T. V. & TSYRYUL'NIKOV, I. S. 2007 Active control of disturbances in a hypersonic shock layer. *Dokl. Phys.* **52** (5), 274–276.
- GAD-EL-HAK, M. 1996 Modern development in flow control. *Appl. Mech. Rev.* **49**, 365–379.
- GAPONOV, S. A. & MASLOV, A. A. 1980 *Evolution of Disturbances in Compressible Flows* (in Russian). Nauka.
- GASTER, M. 2000 Active control of boundary layer instabilities using MEMS. *Curr. Sci.* **79** (6), 774–780.
- HARVEY, W. D. & BUSHNELL, D. M. 1969 Velocity fluctuations intensities in a hypersonic turbulent boundary layer. *AIAA J.* **7** (4), 760–762.
- KEMP, J. H. & OWEN, F. K. 1972 Nozzle wall boundary layer at Mach numbers 20 to 47. *AIAA J.* **10** (7), 872–879.
- KIMMEL, R. L. 2003 Aspects of boundary layer transition control. *Paper 2003-0772*. AIAA.
- KOGAN, M. N. 1969 *Rarefied Gas Dynamics*. Plenum.
- KONTOROVICH, V. M. 1959 Sound reflection and refraction on shock waves (in Russian). *Akust. Zh.* **5**, 314–323.
- KOSINOV, A. D., MASLOV, A. A. & SHEVELKOV, S. G. 1990 Experiments on the stability of supersonic laminar boundary layers. *J. Fluid Mech.* **219**, 621–633.
- KUDRYAVTSEV, A. N. & KHOTYANOVSKY, D. V. 2005 Numerical investigation of high speed free shear flow instability and Mach wave radiation. *Intl J. Aeroacous.* **4** (3 & 4), 267–286.
- KUDRYAVTSEV, A. N., MIRONOV, S. G., POPLAVSKAYA, T. V. & TSYRYUL'NIKOV, I. S. 2006 Experimental study and direct numerical simulation of the evolution of disturbances in a viscous shock layer on a flat plate. *J. Appl. Mech. Tech. Phys.* **47** (5), 617–627.

- LAUFER, J. 1964 Some statistical properties of the pressure field radiated by a turbulent boundary layer. *Phys. Fluids* **7** (8), 1191–1197.
- MA, Y. & ZHONG, X. 2003a Receptivity of a supersonic boundary layer over a flat plate. Part 1. Wave structures and interactions. *J. Fluid Mech.* **488**, 31–78.
- MA, Y. & ZHONG, X. 2003b Receptivity of a supersonic boundary layer over a flat plate. Part 2. Receptivity to free-stream sound. *J. Fluid Mech.* **488**, 79–121.
- MA, Y. & ZHONG, X. 2004 Linear stability and receptivity to free-stream disturbances of a Mach 10. Nonequilibrium reactivity oxygen flow over a flat plate. *Paper* 2004-0256. AIAA.
- MA, Y. & ZHONG, X. 2005 Receptivity of a supersonic boundary layer over a flat plate. Part 3. Effects of different types of free-stream disturbances. *J. Fluid Mech.* **532**, 63–109.
- MACK, L. M. 1975 Linear stability theory and the problem of supersonic boundary-layer transition. *AIAA J.* **13** (3), 278–289.
- MANESH, K., LEE, S., LELE, S. K. & MOIN, P. 1995 The interaction of an isotropic field of acoustic waves with a shock wave. *J. Fluid Mech.* **300**, 383–407.
- MASLOV, A. A., KUDRYAVTSEV, A. N., MIRONOV, S. G., POPLAVSKAYA, T. V. & TSYRYUL'NIKOV, I. S. 2007 Numerical simulation of receptivity of a hypersonic boundary layer to acoustic disturbances. *J. Appl. Mech. Tech. Phys.* **48** (3), 368–374.
- MASLOV, A. A. & MIRONOV, S. G. 1996 Experimental investigation of the hypersonic low-density flow past a half-closed cylindrical cavity. *Fluid Dyn.* **31**, 928–932.
- MASLOV, A. A. & MIRONOV, S. G. 1999 Effect of flow nonparallelism in the shock layer on a flat plate and the angle of on characteristics of density fluctuations (in Russian). *Izv. Ross. Akad. Nauk Mekh. Zhidk. Gaza* **2**, 50–55.
- MASLOV, A. A., MIRONOV, S. G. & ANISKIN, V. M. 2005 Hypersonic shear layer stability experiments. *J. Spacecraft Rockets* **42** (6), 999–1004.
- MASLOV, A. A., MIRONOV, S. G., KUDRYAVTSEV, A. N., POPLAVSKAYA, T. V. & TSYRYUL'NIKOV, I. S. 2008 Controlling the disturbances in a hypersonic flat-plate shock layer by unsteady action from the surface. *Fluid Dyn.* **43** (3), 471–479.
- MASLOV, A. A., MIRONOV, S. G., POPLAVSKAYA, T. V. & SMORODSKY, B. V. 2004a Stability of the hypersonic shock layer on a flat plate. *Fluid Dyn.* **39** (2), 181–188.
- MASLOV, A. A., POPLAVSKAYA, T. V. & SMORODSKY, B. V. 2004b Stability of a hypersonic shock layer on a flat plate. *Compt. Rendus Mec.* **332** (11), 875–880.
- MCKENZIE, J. F. & WESTPHAL, K. O. 1968 Interaction of linear waves with oblique shock waves. *Phys. Fluids* **11**, 2350–2362.
- MIRONOV, S. G. & ANISKIN, V. M. 2004 Experimental study of hypersonic shock layer stability on a circular surface of compression. *Compt. Rendus Mec.* **332** (9), 701–708.
- MIRONOV, S. G. & MASLOV, A. A. 2000a An experimental study of density waves in hypersonic shock layer on a flat plate. *Phys. Fluids* **12** (6), 1544–1553.
- MIRONOV, S. G. & MASLOV, A. A. 2000b Experimental study of secondary instability in a hypersonic shock layer on a flat plate. *J. Fluid Mech.* **412**, 259–277.
- MOREAU, E. 2007 Airflow control by non-thermal plasma. *J. Phys. D* **40**, 605–636.
- MORKOVIN, M. V. 1968 Critical evaluation of transition from laminar to turbulent shear layers with emphasis of hypersonically travelling bodies. *Tech Rep.* 68-149. Air Force Flight Dynamics Laboratory.
- NOSENCHUCK, D. M. 1988 Passive and active control of boundary layer transition. PhD thesis, California Institute of Technology, Pasadena, CA.
- PACK, L. G. & JOSLIN, R. D. 1998 Overview of active control at NASA Langley Research Center. *Tech Rep.* 20040110283. NASA.
- RIST, U. & GMELIN, C. 2006 Active control of laminar-turbulent transition using instantaneous wall vorticity. In *Fifth ERCOFTAC SIG33 Workshop on 'Laminar-Turbulent Transition Mechanisms: Prediction and Control'*, Nasslingen, Stockholm.
- ROGER, K. W., WAINRIGHT, G. B. & TOURYAN, K. J. 1966 Impact and static pressure measurements in high speed flows with transitional Knudsen numbers. In *Rarefied Gas Dynamics* (ed. J. H. deLeeuw) vol. 2, pp. 151–174. Academic.
- SHU, C.-W. & OSHER, S. 1988 Efficient implementation of essentially non-oscillatory shock-capturing schemes. Part I. *J. Comput. Phys.* **77**, 439–471.
- SHU, C.-W. & OSHER, S. 1989 Efficient implementation of essentially non-oscillatory shock-capturing schemes. Part II. *J. Comput. Phys.* **83**, 32–78.

- SMITH, J. A. & DRISCOLL, J. F. 1975 The electron-beam fluorescence technique for measurements in hypersonic turbulent flows. *J. Fluid Mech.* **72** (4), 695–719.
- SURESH, A. & HUYNH, H. T. 1997 Accurate monotonicity-preserving schemes with Runge–Kutta stepping. *J. Comput. Phys.* **136** (Pt 1), 83–99.
- TSYRYUL'NIKOV, I. S. & MIRONOV, S. G. 2005 Wave field of controllable periodic disturbances generated by two sources (in Russian). *Thermophys. Aeromech.* **12** (3), 353–360.
- TUMIN, A. 2006 Receptivity of compressible boundary layers to three-dimensional wall perturbations. *Paper* 2006-1110. AIAA.
- TUMIN, A. 2007 Three-dimensional spatial normal modes in compressible boundary layers. *J. Fluid Mech.* **586**, 295–322.
- TUMIN, A., WANG, X., ZHONG, X. 2007 Direct numerical simulation and the theory of receptivity in a hypersonic boundary layer. *Phys. Fluids* **19** (1), 014101. AIAA.
- WALLACE, J. E. 1969 Hypersonic turbulent boundary layer measurements using an electron-beam. *AIAA J.* **7** (4), 757–759.
- WANG, X. & ZHONG, X. 2005 Receptivity of a Mach 8.0 flow over a sharp wedge with half-angle 5.3° to wall blowing-suction. *Paper* 2005-5025. AIAA.
- WANG, X. & ZHONG, X. 2007 Numerical simulation of hypersonic boundary-layer receptivity to two and three-dimensional wall perturbations. *Paper* 2007-946. AIAA.
- ZANG, T. A., HUSSAINI, M. Y. & BUSHNELL, D. M. 1984 Numerical computations of turbulence amplification in shock-wave interactions. *AIAA J.* **22** (1), 13–21.
- ZHONG, X. 2000 Receptivity of hypersonic boundary layers to free stream disturbances. *Paper* 2000-0531. AIAA.
- ZHONG, X. 2001 Leading-edge receptivity to free stream disturbance waves for hypersonic flow over a parabola. *J. Fluid Mech.* **441**, 315–367.